FLEXURAL - TORSIONAL BUCKLING OF TAPERED MONOSYMMETRIC I BEAM - COLUMNS/TIE - BEAMS

A Thesis Submitted
in Partial Fulfilment of the Requirements
for the Degree of

MASTER OF TECHNOLOGY

by

NILESH H. SHAH

to the

DEPARTMENT OF CIVIL ENGINEERING

INDIAN INSTITUTE OF TECHNOLOGY, KANPUR

AUGUST, 1990

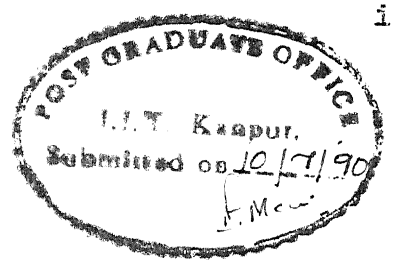

CERTIFICATE

It is certified that the work contained in the thesis entitled **FLEXURAL-TORSIONAL BUCKLING OF TAPERED MONOSYMMETRIC I-BEAM-COLUMNS/TIE-BEAMS**, by Shah Nilesh H., has been carried out under my supervision and that this work has not been submitted elsewhere for a degree.

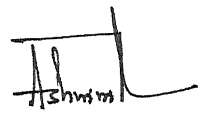

(Ashwini Kumar)
Professor
Department of Civil Engineering
Indian Institute of Technology
Kanpur

July, 1990.

CERTIFICATE

It is certified that the work contained in the thesis entitled **FLEXURAL-TORSIONAL BUCKLING OF TAPERED MONOSYMMETRIC I-BEAM-COLUMNS/TIE-BEAMS**, by Shah Nilesh H., has been carried out under my supervision and that this work has not been submitted elsewhere for a degree.

(Ashwini Kumar)
Professor
Department of Civil Engineering
Indian Institute of Technology
Kanpur

July, 1990.

ABSTRACT

The present investigation deals with flexural-torsional buckling of simply supported, two way linearly tapering, monosymmetric I beam-columns/tie-beams under four types of loading (i) Moment gradient, (ii) Uniformly distributed load, (iii) Single point load, (iv) Two symmetrically placed point loads. In the case of transverse loading, the loads are assumed to be applied at the top flange, at the shear centre or at the bottom flange. Results are presented in either graphical or tabular form. It is shown that the design specifications of IS:800-1984 could be unsafe in predicting the buckling capacity of monosymmetric I beams in some cases.

Dedicated
To

My Parents

ACKNOWLEDGEMENT

I take this opportunity to thank Dr. Ashwini Kumar for his guidance and encouragement during the course of this work.

I am very much thankful to my friends Rajshekhar, Sridhar and Shrikant for their help and co-operation.

Thanks are due to Swami Anand Chaitanya for neat typing and Mr. B.K. Jain for neat sketches.

Nilesh H. Shah

TABLE OF CONTENTS

LIST OF FIGURES

LIST OF TABLES

LIST OF SYMBOLS

A_F : Area of flanges;

A_{Ft}, A_{Fb} : Area of top and bottom flanges respectively;

A_{wz} : Web area at distance z;

[A] : Stiffness matrix;

a : Parameter for position of concentrated load along the span;

a_i : Elements of the stiffness matrix;

$\bar{a}_z$: Load height below shear centre at distance z;

B : Width of the governing flange;

B_t, B_b : Width of top and bottom flanges respectively;

[B] : Load matrix;

b_{ij} : Elements of the stiffness matrix;

d_{ij} : Elements of the load matrix;

E : Young's modulus of elasticity;

e_{ij} : Elements of the stiffness matrix;

e_z : Eccentricity of centroidal axis at distance z;

f_{cb} : Elastic critical buckling stress;

f_i : Elements of the stiffness matrix;

f_y : Yield stress;

g_{ij} : Elements of the load matrix;

h : Distance between flange centroids at centre of the member;

h_i : Elements of the load matrix;

h_w : Height of web at centre of the member;

h_z : Distance between flange centroids at distance z;

I_{xz}, I_{yz} : Major and minor axis second moments of area at

distance z;

I_{yt}, I_{yb} : Second moments of area about section minor axis of top and bottom flanges respectively;

I_{wz} : Warping section constant at distance z;

J_z : Torsion section constant at distance z;

$\bar{K}$: Member parameter defined by Eq. (2.17);

k : Nondimensional buckling moment defined by Eq. (2.17);

L : Half the span of the member;

M : Maximum moment in the member due to externally applied transverse loads;

M_{xz} : Moment about major axis at distance z;

n, $\bar{n}$: Number of terms used in trigonometric series;

P : Axial force: Compression positive, tension negative;

P_E : Euler buckling load;

r_{oz} : Polar radius of gyration about centroid at distance z;

r_z : Polar radius of gyration about shear centre at distance z;

T : Thickness of the governing flange;

T_t, T_b : Thickness of top and bottom flanges respectively;

T_w : Height of web at centre of the member;

U : Strain energy;

u : Lateral deflection of shear centre;

$\bar{u}$: Nondimensional lateral displacement defined by Eq. (2.17);

V : Work done;

W : Concentrated load;

w : Uniformly distributed load;

x,y : Major and minor principal axis respectively;

y_{oz} : Distance between centroid and shear centre at

distance z;

z : Axis along length of the member;

$\bar{z}$: Nondimensional distance along length of the member;

α : Ratio of distance between flange centroids at supports to that at centre of the member;

β : End moment ratio;

γ : Taper parameter;

Δ_r : Co-efficients of the lateral displacement in trigonometric series;

η : Web-flange area ratio at centre of the member (See Eq. 3.1);

η_z : Web-flange area ratio at distance z;

θ_r : Co-efficients of the angle of twist in trigonometric series;

λ : Axial load ratio defined by Eq. (2.17);

μ : Flange area ratio defined by Eq. (2.3);

ρ : Degree of section monosymmetry defined by Eq. (2.2);

ϕ : Angle of twist;

$\bar{\phi}$: Nondimensional angle of twist defined by Eq. (2.17);

CHAPTER I

INTRODUCTION

1.1 STABILITY

The stability of a structure essentially means the stability of its equilibrium configuration or state. In a practical sense, an equilibrium state of a structure or a system is said to be stable if accidental forces, shocks, vibrations, eccentricities, imperfections, inhomogenities or other probable irregularities do not cause the system to depart excessively or disastrously from that state. In a mathematical sense, the stability is usually interpreted to mean that infinitesimal disturbances will cause only infinitesimal departure from the given equilibrium configuration.

The loss of stability under compressive loads is usually termed as structural (or geometric or form) instability, commonly known as buckling. There are three basic ways by which instability can occur in a single structural member:

- Pure flexural buckling about the major principal axis.
- Pure flexural buckling about the minor principal axis.
- Pure torsional buckling about the shear centre axis.

Depending on the sectional properties and external loads, a structural member becomes unstable in any of the above three individual buckling modes or by a combination of these buckling modes. For example, consider a structural member with

monosymmetric I cross section subjected to axial and transverse loads only. The instability can occur by

- Pure flexural buckling about the major principal axis (in-plane buckling).
- Combination of flexural buckling about the minor principal axis and torsional buckling about shear centre axis (flexural-torsional buckling).

The buckling capacity of such a member is the elastic critical load obtained from analysis of above two modes.

1.2 FLEXURAL TORSIONAL BUCKLING

When an I beam is subjected to axial and transverse loads, it may buckle sideways if its compression flange is not laterally supported. It happens because the compression flange, which is in effect like a column on an elastic foundation, becomes unstable. At the critical loading there is a tendency for the compression flange to bend sideways and for the remainder of the cross section to restrain it from doing so. The net effect is that the entire section rotates and moves laterally. Thus, lateral buckling is a combination of twisting and lateral bending brought about by the instability of the compression flange. Therefore, it is termed as flexural-torsional buckling. Since thin walled open sections are most susceptible to such type of buckling, the discussion in subsequent articles will be limited to these shapes, with particular reference to monosymmetric I sections.

The analysis for flexural-torsional buckling is usually based on following assumptions:

- The material is homogeneous, isotropic and elastic.

- Plane sections originally perpendicular to the longitudinal axis of the member, remain plane and perpendicular after bending.
- Flexural deformations are small.

The above three assumptions enable the use of classical beam theory for the purpose of analysis.

- The cross section of the member is allowed to rotate and translate in a plane perpendicular to the longitudinal axis of the member, but no distortions in cross section shape is allowed. (This assumption ignores the effect of local buckling of flanges and web.)
- The beam is initially undistorted and unstressed. (i.e. no geometric imperfactions and no residual stresses.)

Within the limit of above assumptions the buckling capacity of a member depends on the following factors:

- Section properties.
- Loading conditions.
- Lateral restraint provided and its position along the span.
- Displacement, rotational, torsional and warping constraint at the ends.
- Variation in shape of cross-section along the span.

1.3 LITERATURE REVIEW

The elastic flexural-torsional buckling of uniform doubly symmetric members has been studied at length. Numerical solutions and approximate buckling formulae for such members, under various loading and restraint conditions, are available in standard texts

e.g. Timoshenko and Gere (1961), Galambos (1968), Chajes (1974), Trahair and Bradford (1988).

Much of the research work on the buckling of tapered members is focused on doubly symmetric web tapering members. Some early work includes inplane buckling of I sections under axial thrust and axial thrust-end moments combinations with various boundary conditions (Fogel et al 1962; Gore et al 1962 Girijavallabhan 1969). The behaviour of linear and parabolic web tapering cantilever beams under external torque was studied by Lee and Szabo (1967). Culver and Preg (1968) derived differential equation for flexural-torsional buckling of one way web tapering beams and solved it using finite difference method for moment gradient load case. Kitipornchai and trahair (1972, 1975) studied the buckling behaviour of two way tapering members under a central point load. This study also includes effect of variation in the thickness/width. These results were confirmed by Bradford and Cuk (1988) who investigated lateral buckling of monosymmetric I beams using the finite element method. Brown (1981) studied lateral-torsional buckling of two way web tapered I beams. He derived the governing differential equation using energy approach and solved it using finite difference method for central point load.

One of the difficulties encountered in the design of monosymmetric I beams has been the determination of section properties required for calculating the elastic critical moment. Kitipornchai and Trahair (1980) overcame this difficulty by introducing some new parameters. Using these parameters and the energy approach, Kitipornchai et al (1986a, 1986b, 1988a) studied

the buckling of uniform members for various load cases. To simplify the flexural-torsional analysis of beam-columns / tie-beams, Wang and Kitipornchai (1989) proposed a few additional parameters and studied the behaviour of uniform monosymmetric beam-columns/tie-beams under various loading conditions (Kitipornchai and Wang, 1988b).

1.4 AIM OF INVESTIGATION

IS:800 (1984) uses the Merchant Rankine formula to get the maximum permissible bending compressive stress σ_{bc}, for designing a member:

$$\sigma_{bc} = \frac{0.66\, f_{cb}\, f_y}{\left[(f_{cb})^n + (f_y)^n\right]^{1/n}}$$

where f_y is the yield stress of the steel; n is the imperfection factor and f_{cb} is the elastic critical stress in bending. To determine f_{cb} the code proposes a formula or suggests the use of an elastic flexural-torsional buckling analysis. The formula proposed in the code is derived by making use of the equation which is obtained for the elastic critical moment for a simply supported, uniform, monosymmetric, I beam subjected to a constant moment. In actual practice the member can be nonprismatic and the loading can be of any type resulting in various forms of bending moment variations. Under this circumstances one is not sure whether it would be correct to use the formula given in IS:800.

Two way linearly tapering members, which give effective utilization of structural materials, are widely used for plate girders and gantry girders. In such members, only the depth varies along the span while the area of each flange remains constant. With this in view the aim of present investigation is:

- to study the flexural-torsional behaviour of such members under an axial force combined with following external loads:
  * Linear moment gradient.
  * Uniformly distributed load.
  * Single point load placed anywhere on the span.
  * Two symmetrically placed point loads.
- to give values of nondimensional elastic critical moment by means of which f_{cb}, and thus σ_{bc}, can be obtained for sections available in practice.

1.5 OUTLINE OF THESIS

The thesis consists of three chapters. Chapter 1 is the introduction. In chapter 2, all the section properties have been defined. The formulation of the buckling problem for various loading conditions is also given in this chapter. Results of the analysis are presented and discussed in Chapter 3. Whenever possible results obtained from the present analysis are compared with the provisions in IS:800. Tables are presented for doubly symmetric I sections and various loading conditions which can be used for determination of elastic critical stress f_{cb}.

CHAPTER II

PROBLEM FORMULATION

2.1 INTRODUCTION

In this chapter, a general formulation is presented for the flexural-torsional buckling analysis of two way linearly tapering monosymmetric I beam-columns/tie-beams. The method of investigation is similar to that adopted in the recent work of Kritiponchai and Wang (1988b). The various load cases which have been considered in this investigation are shown in Fig. 2.1.

To simplify the analysis, following assumptions are made in addition to those listed in Sec. 1.2:

- Resultant of transverse loads act solely in the vertical plane passing through the shear centre of the section.
- Resultant of axial loads lies in the plane of web. It is parallel to the top flange and acts through the centroid of the section at supports.
- No intermediate lateral restraint is provided.
- The displacements and moments about major and minor axis of the section vanish at the ends of the member. The torsional boundary conditions are, zero twist and zero warping restraint at the ends of the member.
- The flange width, the flange thickness and the web thickness are constant along the span, while the depth varies linearly with maximum value at the centre.
- The angle of tapering is small.

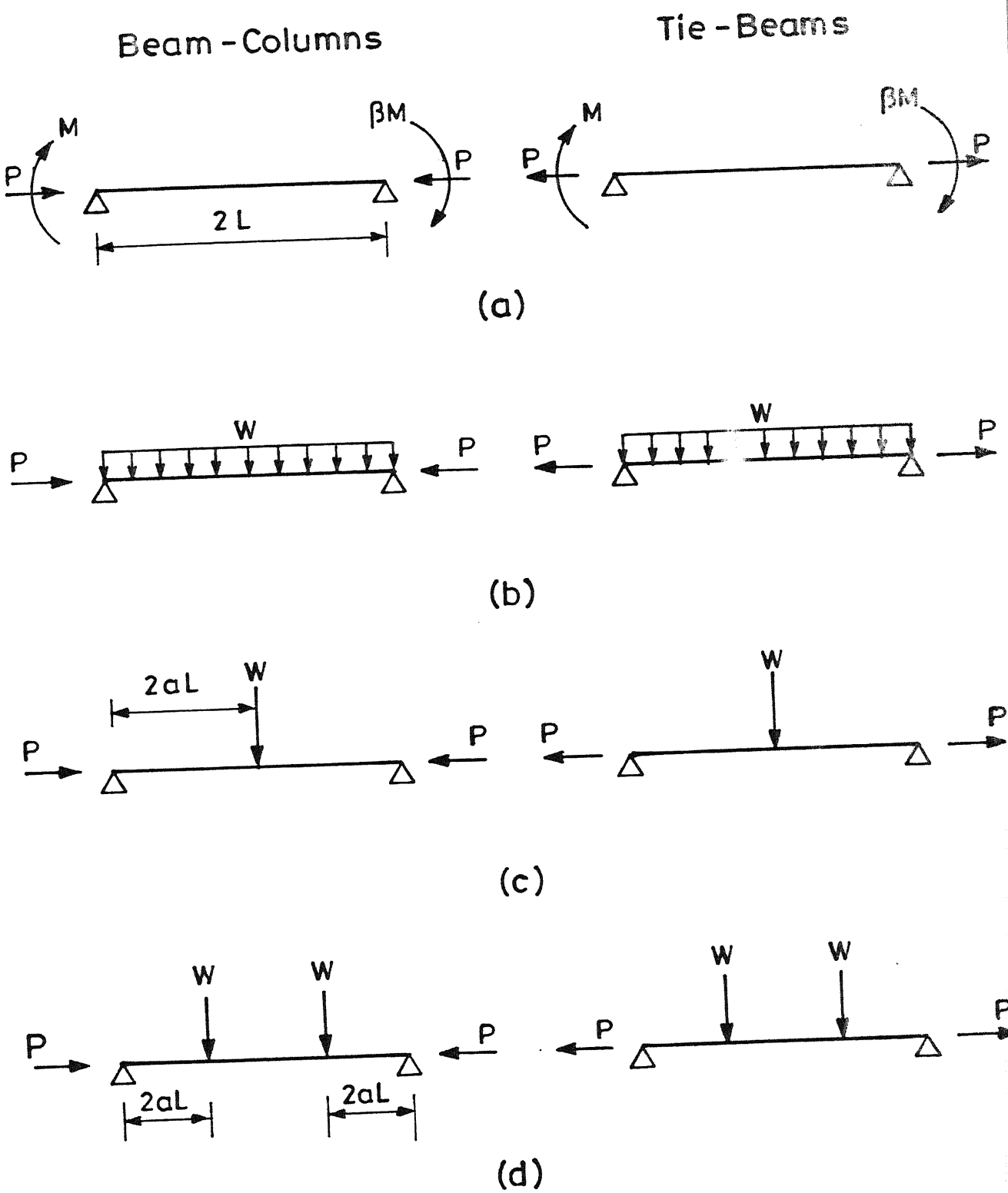

Fig. 2.1 Loading conditions.

A typical structural member with general monosymmetric I-section is shown in Fig. 2.2. The length of the member is 2L. The distance between the flange centroids is αh at the ends and h at the centre. The width and thickness of the top and bottom flanges are designated by B_t, T_t and B_b, T_b, respectively. The origin of the coordinate system is at the left support coinciding with the centroid of the section with z axis along the length of the member and the positive x and the y axis as shown in the figure. The member is assumed simply supported at the ends and unrestrained against warping, i.e. it can freely rotate about the x and y axis at the ends but prevented from rotating about the z axis at these points.

The Rayleigh-Ritz energy method has been used in the analysis. It involves minimizing the total potential energy (which is the sum of the strain energy U, stored in the buckled member and the potential energy V of the external loads) with respect to the buckled shape. We can write the following expression for the strain energy stored in the member when it buckles out of its plane.

$$U = \sum_{i=1,2} \left\{ \frac{1}{2} \int EI_{yzi} \left(\frac{d^2u}{dz^2}\right)^2 dz + \frac{1}{2} \int GJ_{zi} \left(\frac{d\phi}{dz}\right)^2 dz \right.$$

$$\left. + \frac{1}{2} \int EI_{wzi} \left(\frac{d^2\phi}{dz^2}\right)^2 dz \right\} \qquad (2.1)$$

In the above expression u is the lateral displacemenht and ϕ is the angle of twist. The first term on the right hand side represents the strain energy due to bending in the lateral direction, the second term is the contribution due to torsion and the last one is due to warping. The suffix i indicates the portion of member for which the expression is valid. Note that

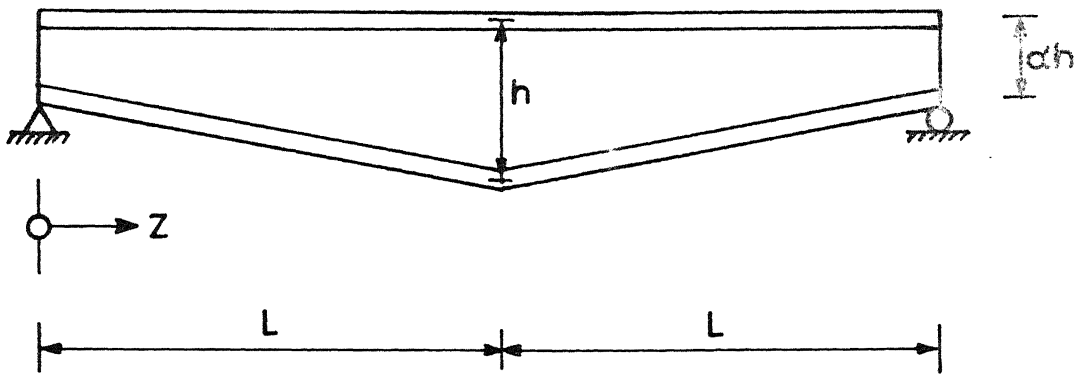

Fig. 2.2 (a): Typical web tapering structural member.

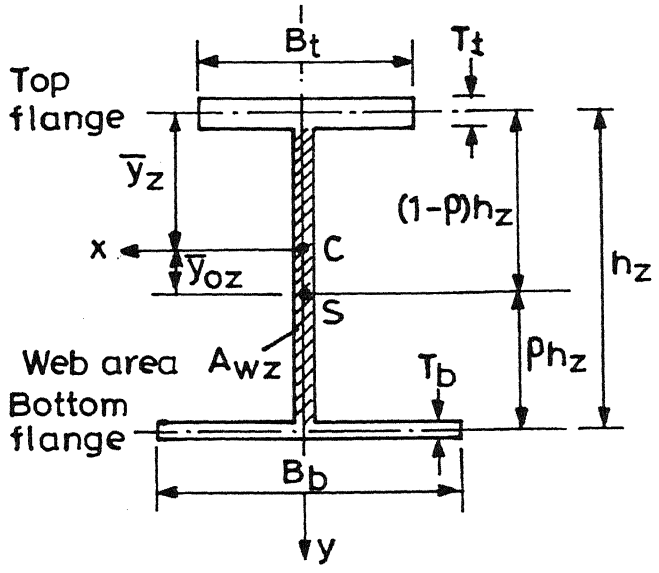

Fig. 2.2 (b) Monosymmetric I-section.

for i = 1, integration limit is 0-L, while for i = 2, integration limit is L-2L.

The expression for the potential energy V for different load cases is given in Sec. 2.3 and 2.4.

2.2 SECTION PROPERTIES

The determination of the section properties required for calculating the elastic critical moment of a monosymmetric section is not straight forward, and the effort required is prohibitive in routine design. Kitipornchai and Trahair (1980) gave following four parameters for prismatic members. These parameters help in simplifying the analysis.

$$\text{(i)}\quad \rho = \frac{I_{yt}}{I_{yt} + I_{yb}} = \frac{I_{yt}}{I_{yo}}\ ; \quad 0 \le \rho \le 1.0 \qquad (2.2)$$

where I_{yt} and I_{yb} are the second moments of area about the y axis, of the top and the bottom flanges, respectively.

$$\text{(ii)}\quad \mu = \frac{A_{Ft}}{A_{Ft} + A_{Fb}} = \frac{A_{Ft}}{A_F}\ ; \quad 0 \le \mu \le 1.0 \qquad (2.3)$$

where A_{Ft} and A_{Fb} are the areas of the top and bottom flanges, respectively. The parameters ρ and μ can be viewed as a measure of the degree of section monosymmetry. Note that $\rho = \mu = 0$ represents an inverted T-section, while $\rho = \mu = 1.0$ denotes a T-section. For a doubly symmetric I section, $\rho = \mu = 0.5$.

(iii) When a monosymmetric section subjected to transverse loads twists during buckling, the major axis moment M_x causes an additional torque which results in an effective change in the member torsional stiffness from GJ to $(GJ + M_x\beta_x)$ in which β_x is the monosymmetry property; the expression for β_x is:

$$\frac{\beta_x}{h} = 0.9\,(2\rho-1)\left[1-\left(\frac{I_y}{I_x}\right)^2\right]$$

or, $\beta_x = 0.9\,(2\rho-1)\,h$, if $I_y << I_x$

For two way tapering members, the above expression can be slightly modified as:

$$\beta_{xzi} = 0.9\,(2\rho-1)\,h_{zi} \qquad i = 1,2 \tag{2.4}$$

where,

$$h_{z1} = \left\{\alpha + (1-\alpha)\frac{z}{L}\right\} h$$

$$h_{z2} = \left\{2 - \alpha - (1-\alpha)\frac{z}{L}\right\} h \tag{2.5}$$

(iv) While the section monosymmetry is represented by ρ, μ and β_{xzi}, the compactness of the section and slenderness of the member is taken care of by the following parameter.

$$\bar{K} = \sqrt{\frac{\pi^2 E I_{yo} h^2}{16\,G J_o L^2}} \tag{2.6}$$

(v) Parameter η_{zi} is defined as the ratio of web area to flange area at any distance z from the origin. It varies linearly along the span and can be written as

$$\eta_{z1} = \left\{\gamma + (1-\gamma)\frac{z}{L}\right\}\eta$$

$$\eta_{z2} = \left\{2 - \gamma + (1-\gamma)\frac{z}{L}\right\}\eta \tag{2.7}$$

where,

$$\gamma = \left(\alpha h - \frac{T_t + T_b}{2}\right) \Big/ \left(h - \frac{T_t + T_b}{2}\right)$$

$$\eta = \mu \left(\frac{T_\omega}{h}\right)\left(\frac{h}{B_t}\right)\left[\frac{h}{T_t} - \frac{1}{2}\left\{1 + \left(\frac{T_b}{h}\right)\left(\frac{h}{T_t}\right)\right\}\right]$$

$$= (1-\mu)\left(\frac{T_\omega}{h}\right)\left(\frac{h}{B_b}\right)\left[\frac{h}{T_b} - \frac{1}{2}\left\{1 + \left(\frac{T_t}{h}\right)\left(\frac{h}{T_b}\right)\right\}\right]$$

Using above parameters, the following useful expressions can be derived:

(vi) Minor axis moment of inertia

$$I_{yzi} = I_{yo}\left[1 + \frac{\eta_{zi}\, T_w^2}{\mu B_t^2 + (1-\mu)\, B_b^2}\right]$$

where,

$$I_{yo} = I_{yt} + I_{yb}.$$

For thin walled members, the second term in the parenthesis can be safely neglected. Then,

$$I_{yzi} = I_{yo} \qquad (2.8)$$

(vii)Torsion constant

$$J_{zi} = J_o\left[1 + \frac{\eta_{zi}\, T_w^2}{\mu T_t^2 + (1-\mu)\, T_b^2}\right] \qquad (2.9)$$

where,

$$J_o = \frac{B_t\, T_t^3}{3} + \frac{B_b\, T_b^3}{3}$$

(viii) Polar radius of gyration about the centroid

$$r_{ozi} = \left[\left\{3\left\{\frac{2\mu+\eta_{zi}}{1+\eta_{zi}}\right\}^2 + \frac{12\mu\,(1-2\mu)}{1+\eta_{zi}}\right\} h_{zi}^2 + \mu B_t^2 + (1-\mu)\, B_b^2 + \eta_{zi}\left(h_{zi} - \frac{T_t+T_b}{2}\right)^2 + n_{zi}\, T_w\right] \Big/ 12\,(1+\eta_{zi})$$

(2.10)

(ix) Distance between centroidal axis and shear centre axis

$$y_{ozi} = \left(\frac{2\mu + \eta_{zi}}{2\,(1 + \eta_{zi})} - \rho \right) h_{zi} \qquad (2.11)$$

(x) Eccentricity of centroidal axis

$$e_{zi} = \left\{ \frac{2\,(1-\mu) + \eta_{zi}}{2\,(1+\eta_{zi})} \right\} h_{zi} - \left\{ \frac{2\,(1-\mu) + \gamma\eta}{2\,(1+\gamma\eta)} \right\} \alpha\, h \qquad (2.12)$$

(xi) Warping section constant

$$I_{wzi} = \rho\,(1-\rho)\, I_{yo}\, h^2_{zi} \qquad (2.13)$$

2.3 MOMENT GRADIENT LOAD CASE

Consider a two way web tapering structural member subjected to moment M at one end and βM at the other end as shown in Fig. 2.1(a).

The expression for the potential energy V of the inplane moment and the axial force when the member buckles out of its plane is given by,

$$V = \sum_{i=1,2} \left\{ \int M_{xzi} \left(\frac{d^2u}{dz^2} \right) \phi \, dz + \frac{1}{2} \int M_{xzi}\, \beta_{xzi} \left(\frac{d\phi}{dz} \right)^2 dz \right.$$
$$\left. - \frac{1}{2} \int P \left[\left(\frac{du}{dz} \right)^2 + r^2_{zi} \left(\frac{d\phi}{dz} \right)^2 - 2y_{ozi} \left(\frac{d^2u}{dz^2} \right) \phi \right] dz \right\} \qquad (2.14)$$

As indicated earlier, the suffix i denotes the portion of member for which the expression is valid; for i = 1 integration limit is 0-L, while for i = 2 it is L-2L. In the expression (2.14), we have,

r^2_{zi} = Polar radius of gyration about shear centre

$$= r_{ozi}^2 + y_{ozi}^2 \qquad (2.15)$$

M_{xzi} = Moment about centroid of the section at any distance z from the origin

$$= M - \frac{(1+\beta)}{2} M \frac{z}{L} + P.e_{zi}$$

$$= M \left[1 - \frac{(1+\beta)}{2} \frac{z}{L} + \frac{P}{M} \left\{ \frac{2(1-\mu)+\eta_{zi}}{2(1+\eta_{zi})} h_{zi} - \frac{2(1-\mu) + \gamma n}{2(1+\gamma\eta)} \alpha h \right\} \right] \qquad (2.16)$$

It is found convenient to use the following nondimensional terms:

$$\bar{u} = \frac{u}{L}; \quad \bar{z} = \frac{z}{L}; \quad \bar{\phi} = \phi \sqrt{\frac{GJ_o}{EI_{yo}}};$$

$$\bar{K} = \sqrt{\frac{\pi^2 EI_{yo}\, h^2}{16\, GJ_o L^2}}; \quad k = \frac{M(2L)}{\sqrt{EI_{yo}\, GJ_o}}; \quad \lambda = \frac{P}{P_E} \qquad (2.17)$$

where,

$$P_E = \frac{\pi^2 EI_{yo}}{4L^2}$$

The total potential energy $\Pi = U + V$ may be non dimensionalized by denoting

$\bar{\Pi} = 2\Pi L / EI_{yo}$, therefore,

$$\bar{\Pi} = \frac{2L}{EI_{yo}} (U + V) \qquad (2.18)$$

Using Eq. (2.1) to (2.17) in Eq. (2.18), the nondimensional expression for total potential energy can be written as:

$$\bar{\Pi} = \int_0^1 \left(1 + \frac{\eta_{z1}}{\mu \left(\frac{T_t}{T_w} \right)^2 + (1-\mu) \left(\frac{T_b}{T_w} \right)^2} \right) \left(\frac{d\bar{\phi}}{d\bar{z}} \right)^2 d\bar{z}$$

$$+ \int_1^2 \left(1 + \frac{\eta_{z2}}{\mu \left(\frac{T_t}{T_w} \right)^2 + (1-\mu) \left(\frac{T_b}{T_w} \right)^2} \right) \left(\frac{d\bar{\phi}}{d\bar{z}} \right)^2 d\bar{z}$$

$$+ \int_0^1 \frac{16\rho(1-\rho)}{\pi^2} \bar{K}^2 \left(\alpha+(1-\alpha)\bar{z}\right)^2 \left(\frac{d^2\bar{\phi}}{d\bar{z}^2}\right)^2 d\bar{z}$$

$$+ \int_1^2 \frac{16\rho(1-\rho)}{\pi^2} \bar{K}^2 \left(2-\alpha-(1-\alpha)\bar{z}\right)^2 \left(\frac{d^2\bar{\phi}}{d\bar{z}^2}\right)^2 d\bar{z}$$

$$+ \int_0^2 \left(\frac{d^2\bar{u}}{d\bar{z}^2} \right)^2 d\bar{z} + \int_0^2 k \left(1 - \frac{1+\beta}{2} \bar{z} \right) \left(\frac{d^2\bar{u}}{d\bar{z}^2} \right) \bar{\phi} \, d\bar{z}$$

$$+ \int_0^1 2\lambda\pi\bar{K} \left\{ 1-\rho - \frac{2(1-\mu)+\gamma\eta}{2(1+\gamma\eta)} \right\} \alpha \left(\frac{d^2\bar{u}}{d\bar{z}^2} \right) \bar{\phi} \, d\bar{z}$$

$$+ \int_1^2 2\lambda\pi\bar{K} \left\{ (1-\rho)(2-\alpha) - \frac{2(1-\mu)+\gamma\eta}{2(1+\gamma\eta)} \alpha \right\} \left(\frac{d^2\bar{u}}{d\bar{z}^2} \right) \bar{\phi} \, d\bar{z}$$

$$+ \int_0^1 2\lambda\pi\bar{K} (1-\rho)(1-\alpha) \bar{z} \left(\frac{d^2\bar{u}}{d\bar{z}^2} \right) \bar{\phi} \, d\bar{z}$$

$$- \int_1^2 2\lambda\pi\bar{K} (1-\rho)(1-\alpha) \bar{z} \left(\frac{d^2\bar{u}}{d\bar{z}^2} \right) \bar{\phi} \, d\bar{z}$$

$$+ \int_0^1 \frac{2k\bar{K}}{\pi} 0.9 (2\rho-1) \left(\alpha+ (1-\alpha) \bar{z}\right) \left[1 - \frac{1+\beta}{2} \bar{z} \right] \left(\frac{d\bar{\phi}}{d\bar{z}} \right)^2 d\bar{z}$$

$$+\int_1^2 \frac{2k\bar{K}}{\pi}\,0.9\,(2\rho-1)\,(2-\alpha-(1-\alpha)\,\bar{z})\left(1-\frac{1+\beta}{2}\,\bar{z}\right)\left(\frac{d\bar{\phi}}{d\bar{z}}\right)^2 d\bar{z}$$

$$+\int_0^1 4\lambda\bar{K}^2\,0.9\,(2\rho-1)\left\{\frac{2(1-\mu)+\eta_{z1}}{2(1+\eta_{z1})}\,(\alpha+(1-\alpha)\,\bar{z})\right.$$

$$\left.-\frac{2(1-\mu)+\gamma\eta}{2(1+\gamma\eta)}\,\alpha\right\}(\alpha+(1-\alpha)\,\bar{z})\left(\frac{d\bar{\phi}}{d\bar{z}}\right)^2 d\bar{z}$$

$$+\int_1^2 4\lambda\bar{K}^2\,0.9\,(2\rho-1)\left\{\frac{2(1-\mu)+\eta_{z2}}{2(1+\eta_{z2})}\,(2-\alpha-(1-\alpha)\,\bar{z})\right.$$

$$\left.-\frac{2(1-\mu)+\gamma\eta}{2(1+\gamma\eta)}\,\alpha\right\}(2-\alpha-(1-\alpha)\,\bar{z})\left(\frac{d\bar{\phi}}{d\bar{z}}\right)^2 d\bar{z}$$

$$-\frac{\lambda\pi^2}{4}\int_0^2\left(\frac{d\bar{u}}{dz}\right)^2-\lambda\int_0^1\frac{\bar{K}^2}{3(1+\eta_{z1})}\left[\left\{3\left(\frac{2\mu+\eta_{z1}}{1+\eta_{z1}}\right)^2\right.\right.$$

$$+\frac{12\mu(1-2\mu)}{1+\eta_{z1}}+\frac{3(2\mu-2\rho+\eta_{z1}(1-2\rho))^2}{1+\eta_{z1}}+\eta_{z1}\Big\}(\alpha+(1-\alpha)\bar{z})^2$$

$$\left.+\mu\left(\frac{B_t}{h}\right)^2+(1-\mu)\left(\frac{B_b}{h}\right)^2-\eta_{z1}\left(\frac{T_t+T_b}{h}\right)(\alpha+(1-\alpha)\bar{z})\right]$$

$$\left(\frac{d\bar{\phi}}{d\bar{z}}\right)^2 d\bar{z}-\lambda\int_1^2\frac{\bar{K}^2}{3(1+\eta_{z2})}\left[\left\{3\left(\frac{2\mu+\eta_{z2}}{1+\eta_{z2}}\right)^2\right.\right.$$

$$+\frac{12\mu(1-2\mu)}{1+\eta_{z2}}+\frac{3(2\mu-2\rho+\eta_{z2}(1-2\rho))^2}{1+\eta_{z2}}+\eta_{z2}\Big\}(2-\alpha-(1-\alpha)\bar{z})^2$$

$$\left.+\mu\left(\frac{B_t}{h}\right)^2+(1-\mu)\left(\frac{B_b}{h}\right)^2-\eta_{z2}\left(\frac{T_t+T_b}{h}\right)(2-\alpha-(1-\alpha)\bar{z})\right]$$

$$\left(\frac{d\bar{\phi}}{d\bar{z}}\right)^2 d\bar{z} \qquad (2.19)$$

As mentioned in Sec. 2.1, the boundary conditions are:

$$\bar{u} = \frac{d^2\bar{u}}{d\bar{z}^2} = 0 \quad \text{at} \quad \bar{z} = 0,\ 2.0$$

i.e. the displacement and the moment vanish at the ends of the member.

$$\bar{\phi} = \frac{d^2\bar{\phi}}{d\bar{z}^2} = 0 \quad \text{at} \quad \bar{z} = 0,\ 2.0$$

which imply zero twist and zero warping restraint at the ends of the member.

In view of the boundary conditions mentioned above, the nondimensional displacement and rotation functions, $\bar{u}$ and $\bar{\phi}$, may be parameterized by the following trigonometric series.

$$\bar{u} = \sum_{r=1}^{n} \Delta_r \sin\frac{\pi r\bar{z}}{2}; \qquad \bar{\phi} = \sum_{r=1}^{\bar{n}} \theta_r \sin\frac{\pi \bar{r}\bar{z}}{2}; \qquad (2.20)$$

The Rayleigh–Ritz method requires

$$\frac{\partial\bar{\Pi}}{\partial\Delta_r} = 0, \qquad r = 1, \ldots, n$$

$$\frac{\partial\bar{\Pi}}{\partial\theta_r} = 0, \qquad \bar{r} = 1, \ldots, \bar{n}$$

Substituting the relation (2.20) in the expression (2.19) and performing above operations, we get the following two Ritz equations.

$$\sum_{r=1}^{n} \frac{r^2\pi^2}{2}\left[\int_0^2 r^2 \sin^2\frac{\pi r\bar{z}}{2} - \int_0^2 \lambda \cos^2\frac{\pi r\bar{z}}{2}\, d\bar{z}\right]\Delta_r + \sum_{r=1}^{n}\sum_{\bar{r}=1}^{\bar{n}} r^2$$

$$(-2\lambda\pi\bar{K})\left[\int_0^1 \alpha\left\{1-\rho - \frac{2(1-\mu)+\gamma\eta}{2(1+\gamma\eta)}\right\}\sin\frac{\pi r\bar{z}}{2}\sin\frac{\pi\bar{r}\bar{z}}{2}\, d\bar{z}\right.$$

$$+ \int_{1}^{2} \left\{ (1-\rho)\ (2-\alpha) - \frac{2(1-\mu)+\gamma\eta}{2(1+\gamma\eta)}\ \alpha \right\} \sin \frac{\pi r \bar{z}}{2} \sin \frac{\pi \bar{r} \bar{z}}{2}\ d\bar{z}$$

$$+ \int_{0}^{1} (1-\rho)\ (1-\alpha)\ \bar{z} \sin \frac{\pi r \bar{z}}{2} \sin \frac{\pi \bar{r} \bar{z}}{2}\ d\bar{z} - \int_{1}^{2} (1-\rho)\ (1-\alpha)\ \bar{z} \sin \frac{\pi r \bar{z}}{2}$$

$$\sin \frac{\pi \bar{r} \bar{z}}{2}\ d\bar{z} \Big] \theta_{\bar{r}} = k \sum_{r=1}^{n} \sum_{r=1}^{\bar{n}} \left[r^2 \int_{0}^{2} \left\{ 1 - \frac{1+\beta}{2}\ \bar{z} \right\} \right.$$

$$\left. \sin \frac{\pi r \bar{z}}{2} \sin \frac{\pi \bar{r} \bar{z}}{2}\ d\bar{z} \right] \theta_{\bar{r}} \qquad (2.21)$$

$$\sum_{r=1}^{n} \sum_{r=1}^{\bar{n}} (-2\lambda\pi\bar{K})\ r^2 \left[\int_{0}^{1} \alpha \left\{ 1-\rho - \frac{2(1-\mu)+\gamma\eta}{2(1+\gamma\eta)} \right\} \sin \frac{\pi r \bar{z}}{2} \sin \frac{\pi \bar{r} \bar{z}}{2}\ d\bar{z} \right.$$

$$+ \int_{1}^{2} \left\{ (1-\rho)\ (2-\alpha) - \frac{2(1-\mu)+\gamma\eta}{2(1+\gamma\eta)}\ \alpha \right\} \sin \frac{\pi r \bar{z}}{2} \sin \frac{\pi \bar{r} \bar{z}}{2}\ d\bar{z}$$

$$+ \int_{0}^{1} (1-\rho)\ (1-\alpha)\ \bar{z} \sin \frac{\pi r \bar{z}}{2} \sin \frac{\pi \bar{r} \bar{z}}{2}\ d\bar{z} - \int_{1}^{2} (1-\rho)\ (1-\alpha)\ \bar{z} \sin \frac{\pi r \bar{z}}{2}$$

$$\left. \sin \frac{\pi \bar{r} \bar{z}}{2}\ d\bar{z} \right] \Delta_r + \sum_{r=1}^{n} \sum_{r=1}^{\bar{n}} 2\bar{r}^2 \left[\int_{0}^{1} \left[1 + \frac{\eta_{z1}}{\mu \left(\frac{T_t}{T_w} \right)^2 + (1-\mu) \left(\frac{T_b}{T_w} \right)^2} \right] \right.$$

$$\left. \cos \frac{\pi r \bar{z}}{2} \cos \frac{\pi \bar{r} \bar{z}}{2}\ d\bar{z} + \int_{1}^{2} \left[1 + \frac{\eta_{z2}}{\mu \left(\frac{T_t}{T_w} \right)^2 + (1-\mu) \left(\frac{T_b}{T_w} \right)^2} \right] \right]$$

$$\cos\frac{\pi r\bar{z}}{2}\cos\frac{\pi\bar{r}\bar{z}}{2}\,d\bar{z} + \int_0^1 4\rho\,(1-\rho)\bar{K}^2\,\bar{r}^2\,(\alpha+(1-\alpha)\bar{z})^2\sin\frac{\pi r\bar{z}}{2}\sin\frac{\pi\bar{r}\bar{z}}{2}\,d\bar{z}$$

$$+\int_1^2 4\rho\,(1-\rho)\bar{K}^2\,\bar{r}^2\,(2-\alpha-(1-\alpha)\bar{z})^2\sin\frac{\pi r\bar{z}}{2}\sin\frac{\pi\bar{r}\bar{z}}{2}\,d\bar{z}$$

$$+\int_0^1 3.6\lambda\bar{K}^2\,(2\rho-1)\left\{\frac{2(1-\mu)+\eta_{z1}}{2(1+\eta_{z1})}\,(\alpha+(1-\alpha)\,\bar{z}) - \frac{2(1-\mu)+\gamma\eta}{2(1+\gamma\eta)}\,\alpha\right\}$$

$$(\alpha+(1-\alpha)\,\bar{z})\cos\frac{\pi r\bar{z}}{2}\cos\frac{\pi\bar{r}\bar{z}}{2}\,d\bar{z} + \int_1^2 3.6\lambda\bar{K}^2\,(2\rho-1)\left\{\frac{2(1-\mu)+\eta_{z2}}{2(1+\eta_{z2})}\right.$$

$$\left.(2-\alpha-(1-\alpha)\,\bar{z}) - \frac{2(1-\mu)+\gamma\eta}{2(1+\gamma\eta)}\,\alpha\right\}(2-\alpha-(1-\alpha)\,\bar{z})\cos\frac{\pi r\bar{z}}{2}\cos\frac{\pi\bar{r}\bar{z}}{2}\,d\bar{z}$$

$$-\int_0^1 \frac{\lambda\bar{K}^2}{3(1+\eta_{z1})}\left[\left\{3\left(\frac{2\mu+\eta_{z1}}{1+\eta_{z1}}\right)^2 + \frac{12\mu(1-2\mu)}{1+\eta_{z1}} + \frac{3(2\mu-2\rho+\eta_{z1}\,(1-2\rho))^2}{1+\eta_{z1}}\right.\right.$$

$$\left.\left.+\eta_{z1}\right\}(\alpha+(1-\alpha)\bar{z})^2 + \mu\left(\frac{B_t}{h}\right)^2 + (1-\mu)\left(\frac{B_b}{h}\right)^2 - \eta_{z1}\left(\frac{T_t+T_b}{h}\right)(\alpha+(1-\alpha)\bar{z})\right]$$

$$\cos\frac{\pi r\bar{z}}{2}\cos\frac{\pi\bar{r}\bar{z}}{2}\,d\bar{z} - \int_1^2 \frac{\lambda\bar{K}^2}{3(1+\eta_{z2})}\left[\left\{3\left(\frac{2\mu+\eta_{z2}}{1+\eta_{z2}}\right)^2 + \frac{12\mu(1-2\mu)}{1+\eta_{z2}}\right.\right.$$

$$\left.\left.+\frac{3(2\mu-2\rho+\eta_{z2}\,(1-2\rho))^2}{1+\eta_{z2}} + \eta_{z2}\right\}(2-\alpha-(1-\alpha)\bar{z})^2 + \mu\left(\frac{B_t}{h}\right)^2\right.$$

$$+ (1-\mu)\left(\frac{B_b}{h}\right)^2 - \eta_{z2}\left(\frac{T_t+T_b}{h}\right)(2-\alpha-(1-\alpha)\bar{z})\Big] \cos\frac{\pi r\bar{z}}{2} \cos\frac{\pi \bar{r}\bar{z}}{2}\, d\bar{z} \Big] \theta_{\bar{r}}$$

$$= k \sum_{r=1}^{n} \sum_{\bar{r}=1}^{\bar{n}} r^2 \left[\int_0^2 \left[1 - \frac{1+\beta}{2} \bar{z} \right] \sin\frac{\pi r\bar{z}}{2} \sin\frac{\pi \bar{r}\bar{z}}{2}\, d\bar{z} \right] \Delta_r$$

$$+ k \sum_{r=1}^{n} \sum_{\bar{r}=1}^{\bar{n}} r\, \bar{r}\, \frac{(-3.6\, \bar{K}\, (2\rho - 1))}{\pi} \left[\int_0^1 (\alpha+(1-\alpha)\bar{z}) \left[1 - \frac{1+\beta}{2} \bar{z} \right] \right.$$

$$\cos\frac{\pi r\bar{z}}{2} \cos\frac{\pi \bar{r}\bar{z}}{2}\, d\bar{z} + \int_1^2 (2-\alpha-(1-\alpha)\bar{z}) \left[1 - \frac{1+\beta}{2} \bar{z} \right]$$

$$\left. \cos\frac{\pi r\bar{z}}{2} \cos\frac{\pi \bar{r}\bar{z}}{2}\, d\bar{z} \right] \theta_{\bar{r}} \qquad (2.22)$$

In matrix form, the preceding two equations can be written as:

$$\begin{bmatrix}
a_1 & 0 & 0 & b_{11} & b_{12} & b_{1\bar{n}} \\
0 & 0 & 0 & b_{21} & b_{22} & b_{2\bar{n}} \\
\cdot & \cdot & \cdot & \cdot & \cdot & \cdot \\
0 & 0 & a_n & b_{n1} & b_{n2} & b_{n\bar{n}} \\
e_{11} & e_{12} & e_{1n} & f_{11} & f_{12} & f_{1\bar{n}} \\
e_{21} & e_{22} & e_{2n} & f_{21} & f_{22} & f_{2\bar{n}} \\
\cdot & \cdot & \cdot & \cdot & \cdot & \cdot \\
e_{\bar{n}1} & e_{\bar{n}2} & e_{\bar{n}n} & f_{\bar{n}1} & f_{\bar{n}2} & f_{\bar{n}\bar{n}}
\end{bmatrix}
\begin{Bmatrix}
\Delta_1 \\ \Delta_2 \\ \cdot \\ \Delta_n \\ \theta_1 \\ \theta_2 \\ \cdot \\ \theta_{\bar{n}}
\end{Bmatrix}$$

$$= k \begin{bmatrix} 0 & 0 & 0 & d_{11} & d_{12} & d_{1\bar{n}} \\ 0 & 0 & 0 & d_{21} & d_{22} & d_{2\bar{n}} \\ . & . & . & . & . & . \\ 0 & 0 & 0 & d_{n1} & d_{n2} & d_{n\bar{n}} \\ g_{11} & g_{12} & g_{1n} & h_{11} & h_{12} & h_{1\bar{n}} \\ g_{21} & g_{22} & g_{2n} & h_{21} & h_{22} & h_{2\bar{n}} \\ . & . & . & . & . & . \\ g_{\bar{n}1} & g_{\bar{n}2} & g_{\bar{n}n} & h_{\bar{n}1} & h_{\bar{n}2} & h_{\bar{n}\bar{n}} \end{bmatrix} \begin{Bmatrix} \Delta_1 \\ \Delta_2 \\ . \\ \Delta_n \\ \theta_1 \\ \theta_2 \\ . \\ \theta_{\bar{n}} \end{Bmatrix} \qquad (2.23$$

or in short, $[\ A\ ]\ \{\ X\ \} = k\ [\ B\ ]\ \{\ X\ \}$

where, $[\ A\ ]$ is the stiffness matrix and $[\ B\ ]$ is the load matrix.

The elements of matrices $[\ A\ ]$ and $[\ B\ ]$ are:

$$a_i = \frac{\pi^2 i^2}{2} [\ i^2 - \lambda\ ]; \quad i = 1, 2, \ldots, n. \qquad (2.24)$$

$$b_{ij} = e_{ji} = (-2\lambda\pi\bar{K})\ i^2 \left[(1-\rho) - \frac{2(1-\mu)+\gamma\eta}{2(1+\gamma\eta)} - (1-\rho)(1-\alpha)\left\{ \frac{1}{2} + \frac{1}{\pi^2 i^2} (\cos \pi i - 1) \right\} \right] ; \ i=j$$

$$= \frac{-4\lambda\bar{K}\ (1-\rho)(1-\alpha)\ i^2}{\pi} \left(\frac{1-\cos(i+j)\pi+2(-1)^{i+j}-2\cos(i+j)\pi/2}{(i+j)^2} - \frac{1-\cos(i-j)\pi+2(-1)^{i+j}-2\cos(i-j)\pi/2}{(i-j)^2} \right) ; \ i \neq j$$

where, $i = 1, \ldots, n;\ j = 1, \ldots, \bar{n}.$ (2.25)

$$d_{ij} = g_{ji} = i^2 \frac{(1-\beta)}{2} ; \quad i = j$$

$$= -i^2 \frac{(1+\beta)}{\pi^2} \left(\frac{1-\cos\ (i+j)\ \pi}{(i+j)^2} - \frac{1-\cos\ (i-j)\ \pi}{(i-j)^2} \right) ; \ i \neq j$$

where, $i = 1, \ldots, n;\ j = 1, \ldots, \bar{n}.$ (2.26)

$$f_{ij} = 2i^2 \left\{ \int_0^1 \left[1 + \frac{\eta_{z1}}{\mu \left(\frac{T_t}{T_w} \right)^2 + (1-\mu) \left(\frac{T_b}{T_w} \right)^2} \right] \cos \frac{\pi i \bar{z}}{2} \cos \frac{\pi j \bar{z}}{2} \, d\bar{z} \right.$$

$$+ \int_1^2 \left[1 + \frac{\eta_{z2}}{\mu \left(\frac{T_t}{T_w} \right)^2 + (1-\mu) \left(\frac{T_b}{T_w} \right)^2} \right] \cos \frac{\pi i \bar{z}}{2} \cos \frac{\pi j \bar{z}}{2} \, d\bar{z}$$

$$+ \int_0^1 4\rho \, (1-\rho) \bar{K}^2 \, i^2 \, (\alpha + (1-\alpha)\bar{z})^2 \sin \frac{\pi i \bar{z}}{2} \sin \frac{\pi j \bar{z}}{2} \, d\bar{z}$$

$$+ \int_1^2 4\rho \, (1-\rho) \bar{K}^2 \, i^2 \, (2-\alpha-(1-\alpha)\bar{z})^2 \sin \frac{\pi i \bar{z}}{2} \sin \frac{\pi j \bar{z}}{2} \, d\bar{z}$$

$$+ \int_0^1 3.6\lambda \bar{K}^2 \, (2\rho-1) \left\{ \frac{2(1-\mu)+\eta_{z1}}{2(1+\eta_{z1})} \, (\alpha + (1-\alpha)\, \bar{z}) - \frac{2(1-\mu)+\gamma\eta}{2(1+\gamma\eta)} \, \alpha \right\}$$

$$(\alpha + (1-\alpha)\, \bar{z}) \cos \frac{\pi i \bar{z}}{2} \cos \frac{\pi j \bar{z}}{2} \, d\bar{z} + \int_1^2 3.6\lambda \bar{K}^2 \, (2\rho-1)$$

$$\left\{ \frac{2(1-\mu)+\eta_{z2}}{2(1+\eta_{z2})} \, (2-\alpha - (1-\alpha)\, \bar{z}) - \frac{2(1-\mu)+\gamma\eta}{2(1+\gamma\eta)} \, \alpha \right\}$$

$$(2-\alpha-(1-\alpha)\, \bar{z}) \cos \frac{\pi i \bar{z}}{2} \cos \frac{\pi j \bar{z}}{2} \, d\bar{z}$$

$$- \int_0^1 \frac{\lambda \bar{K}^2}{3(1+\eta_{z1})} \left\{ \left\{ 3 \left[\frac{2\mu+\eta_{z1}}{1+\eta_{z1}} \right]^2 + \frac{12\mu(1-2\mu)}{1+\eta_{z1}} \right.\right.$$

$$\left.\left. + \frac{3(2\mu-2\rho+\eta_{z1}\,(1-2\rho))^2}{1+\eta_{z1}} + \eta_{z1} \right\} (\alpha+(1-\alpha)\bar{z})^2 + \mu \left(\frac{B_t}{h} \right)^2 \right.$$

$$+ (1-\mu)\left(\frac{B_b}{h}\right)^2 - \eta_{z1}\left(\frac{T_t+T_b}{h}\right)(\alpha+(1-\alpha)\bar{z})\Big] \cos\frac{\pi i\bar{z}}{2} \cos\frac{\pi j\bar{z}}{2}\, d\bar{z}$$

$$- \int_1^2 \frac{\lambda\bar{K}^2}{3(1+\eta_{z2})} \Bigg[\Bigg\{ 3\left[\frac{2\mu+\eta_{z2}}{1+\eta_{z2}}\right]^2 + \frac{12\mu(1-2\mu)}{1+\eta_{z2}}$$

$$+ \frac{3(2\mu-2\rho+\eta_{z2}(1-2\rho))^2}{1+\eta_{z2}} + \eta_{z2}\Bigg\}(2-\alpha-(1-\alpha)\bar{z})^2 + \mu\left(\frac{B_t}{h}\right)^2$$

$$+ (1-\mu)\left(\frac{B_b}{h}\right)^2 - \eta_{z2}\left(\frac{T_t+T_b}{h}\right)(2-\alpha-(1-\alpha)\bar{z})\Big] \cos\frac{\pi i\bar{z}}{2} \cos\frac{\pi j\bar{z}}{2}\, d\bar{z} \Bigg]$$

where, $i = 1, \ldots, \bar{n}$; $j = 1, \ldots, \bar{n}$. (2.27)

$$h_{ij} = ij\,\frac{(-3.6\,\bar{K}\,(2\rho-1))}{\pi}\Bigg[\int_0^1 (\alpha+(1-\alpha)\bar{z})\left(1-\frac{1+\beta}{2}\bar{z}\right)$$

$$\cos\frac{\pi i\bar{z}}{2} \cos\frac{\pi j\bar{z}}{2}\, d\bar{z} + \int_1^2 (2-\alpha-(1-\alpha)\bar{z})\left(1-\frac{1+\beta}{2}\bar{z}\right)$$

$$\cos\frac{\pi i\bar{z}}{2} \cos\frac{\pi j\bar{z}}{2}\, d\bar{z}\Bigg];$$

where, $i = 1, \ldots, \bar{n}$; $j = 1, \ldots, \bar{n}$. (2.28)

A nontrival solution of Eq. (2.23) exists when,

$$| [A] - k [B] | = 0$$

This yields a power series of order $(n + \bar{n})$ whose lowest possible root is the critical value of the buckling parameter k. Sufficient number of terms (n and $\bar{n}$) in the trigonometric series (Eq. 2.20) must be taken for accurate results.

2.4 TRANSVERSE LOAD CASES

Following the procedure outlined in the previous section, elements of the stiffness matrix [A] and the load matrix [B] can be obtained for load conditions shown in Figs. 2.1 (b,c,d). In each load cases, following load positions are analysed:

- Top flange loading
- Shear centre loading
- Bottom flange loading

At this stage it is necessary to define a parameter $\bar{a}_{zi}$, which describes the load height below shear centre. The values of $\bar{a}_{zi}$ are listed below:

$$\bar{a}_{zi} = \begin{cases} -(1-\rho)\, h_{zi} & ; \text{ top flange loading (TF)} \\ 0 & ; \text{ shear centre loading (SC)} \\ \rho h_{zi} & ; \text{ bottom flange loading (BF)} \end{cases} \qquad (2.29)$$

The elements of the matrix [A] depend on the geometry of the structural member, material properties and the axial load. Therefore, the matrix [A] will remain the same for all transverse load cases. On the other hand, the matrix [B] will change with loading conditions.

Instead of writing each step, only those expressions, which change with loading conditions/load positions are given below.

2.4.1 Uniformly Distributed Load

$$V = \sum_{i=1,2} \left\{ \int M_{xzi} \left(\frac{d^2u}{dz^2} \right) \phi \, dz + \frac{1}{2} \int M_{xzi}\, \beta_{xzi} \left(\frac{d\phi}{dz} \right)^2 dz \right.$$

$$\left. - \frac{1}{2} \int P \left[\left(\frac{du}{dz} \right)^2 + r_{zi}^2 \left(\frac{d\phi}{dz} \right)^2 - 2y_{ozi} \left(\frac{d^2u}{dz^2} \right) \phi \right] dz \right.$$

$$+ \frac{1}{2} \int w \bar{a}_{zi} \phi^2 \, dz \Big\} \qquad (2.30)$$

$$M_{xzi} = M \left[2 \frac{z}{L} - \left(\frac{z}{L} \right)^2 + \frac{P}{M} e_{zi} \right] \qquad (2.31)$$

where, $M = wL^2/2$ and e_{zi} is given by Eq. (2.12).

$$d_{ij} = g_{ji} = 2i^2/3 + 2/n^2; \quad i = j$$

$$= \frac{4i^2}{n^2} \left[\frac{1+\cos (i+j) n}{(i+j)^2} - \frac{1+\cos (i-j) n}{(i-j)^2} \right] ; \quad i \neq j$$

where, $i = 1, \ldots, n; \; j = 1, \ldots, \bar{n}.$ (2.32)

$$h_{ij} = ij \frac{(-3.6 \bar{K} (2\rho - 1))}{n} \left[\int_0^1 (\alpha+(1-\alpha)\bar{z}) \; (2\bar{z} - \bar{z}^2) \right.$$

$$\cos \frac{n i \bar{z}}{2} \cos \frac{n j \bar{z}}{2} \, d\bar{z} + \int_1^2 (2-\alpha-(1-\alpha)\bar{z}) \; (2\bar{z} - \bar{z}^2)$$

$$\left. \cos \frac{n i \bar{z}}{2} \cos \frac{n j \bar{z}}{2} \, d\bar{z} \right] - \frac{32\bar{K}}{n^3} \left(\frac{\bar{a}_{zi}}{h_{zi}} \right) \left[\int_0^1 (\alpha+(1-\alpha)\bar{z}) \right.$$

$$\left. \sin \frac{n i \bar{z}}{2} \sin \frac{n j \bar{z}}{2} \, d\bar{z} + \int_1^2 (2-\alpha-(1-\alpha)\bar{z}) \sin \frac{n i \bar{z}}{2} \sin \frac{n j \bar{z}}{2} \, d\bar{z} \right]$$

where, $i = 1, \ldots, \bar{n}; \quad j = 1, \ldots, \bar{n}.$ (2.33)

It may be noted that $\bar{a}_{zi}/h_{si})$ is a constant and its value is given by Eq. (2.28).

2.4.2 Single Point Load

$$V = \sum_{i=1,2} \left\{ \int M_{xzi} \left(\frac{d^2u}{dz^2} \right) \phi \, dz + \frac{1}{2} \int M_{xzi} \beta_{xzi} \left(\frac{d\phi}{dz} \right)^2 dz \right.$$

$$\left. - \frac{1}{2} \int P \left[\left(\frac{du}{dz} \right)^2 + r_{zi}^2 \left(\frac{d\phi}{dz} \right)^2 - 2y_{ozi} \left(\frac{d^2u}{dz^2} \right) \phi \right] dz \right\}$$

$$+ \frac{1}{2} W \bar{a}_{z1} \phi^2 \Big|_{z=2aL} \qquad (2.34)$$

$$M_{xz1} = M \left(\frac{z}{2aL} + \frac{P}{M} e_{z1} \right), \; 0 \le \frac{z}{L} \le 2a$$

$$M \left(\frac{2-z/L}{2(1-a)} + \frac{P}{M} e_{z1} \right), \; 2a \le \frac{z}{L} \le 1.0$$

$$M_{xz2} = M \left(\frac{2-z/L}{2(1-a)} + \frac{P}{M} e_{z2} \right), \; 1.0 \le \frac{z}{L} \le 2.0 \qquad (2.35)$$

where, $M = 2Wa\,(1-a)L$

$$d_{ij} = i^2 \left(\frac{1}{2} + \frac{1-\cos 2\pi ia}{4\pi^2 i^2 a(1-a)} \right) ; \quad i = j$$

$$= \frac{i^2}{a\pi^2} \left(\frac{1+ \{a/(1-a)\} \cos (i+j)\pi - \{1/(1-a)\} \cos(i+j)\pi a}{(i+j)^2} \right.$$

$$\left. - \frac{1+ \{a/(1-a)\} \cos (i-j)\pi - \{1/(1-a)\} \cos(i-j)\pi a}{(i-j)^2} \right); \; i \neq$$

where, $i = 1, \ldots, n$; $j = 1, \ldots, \bar{n}$. (2.36)

$$h_{ij} = ij \frac{(-3.6 \bar{K} (2\rho - 1))}{\pi} \left(\int_0^{2a} (\alpha+(1-\alpha)\bar{z}) \frac{\bar{z}}{2a} \right.$$

$$\cos \frac{\pi i \bar{z}}{2} \cos \frac{\pi j \bar{z}}{2} d\bar{z} + \int_{2a}^{1} (\alpha+(1-\alpha)\bar{z}) \frac{(2-\bar{z})}{2(1-a)}$$

$$\cos \frac{\pi i \bar{z}}{2} \cos \frac{\pi j \bar{z}}{2} d\bar{z} + \int_{1}^{2} (2-\alpha-(1-\alpha)\bar{z}) \frac{(2-\bar{z})}{2(1-a)}$$

$$\left. \cos \frac{\pi i \bar{z}}{2} \cos \frac{\pi j \bar{z}}{2} d\bar{z} \right) - \frac{8\bar{K}}{\pi^3 a\,(1-a)} \left(\frac{\bar{a}_{zi}}{h_{zi}} \right) \left\{ (\alpha+2a(1-\alpha)) \right.$$

$$\left. \sin \pi ia \sin \pi ja \right\};$$

where, $i = 1, \ldots, \bar{n}$; $j = 1, \ldots, \bar{n}$. (2.37)

2.4.3 Two Point Load

$$V = \sum_{i=1,2} \left\{ \int M_{xzi} \left(\frac{d^2u}{dz^2} \right) \phi \, dz + \frac{1}{2} \int M_{xzi} \beta_{xzi} \left(\frac{d\phi}{dz} \right)^2 dz \right.$$

$$\left. - \frac{1}{2} \int P \left[\left(\frac{du}{dz} \right)^2 + r_{zi}^2 \left(\frac{d\phi}{dz} \right)^2 - 2y_{ozi} \left(\frac{d^2u}{dz^2} \right) \phi \right] dz \right\}$$

$$+ \frac{1}{2} W \bar{a}_{z1} \phi^2 \Big|_{z=2aL} + \frac{1}{2} W \bar{a}_{z2} \phi^2 \Big|_{z=2(1-a)L} \qquad (2.38)$$

$$M_{xz1} = M \left(\frac{z}{2aL} + \frac{P}{M} e_{z1} \right), \quad 0 \le \frac{z}{L} \le 2a$$

$$= M \left(1 + \frac{P}{M} e_{z1} \right), \quad 2a \le \frac{z}{L} \le 1.0$$

$$M_{xz2} = M \left(1 + \frac{P}{M} e_{z2} \right), \quad 1.0 \le \frac{z}{L} \le 2(1-a)$$

$$= M \left(\frac{1}{a} \left\{ 1 - \frac{z}{2L} \right\} + \frac{P}{M} e_{z2} \right), \quad 2(1-a) \le \frac{z}{L} \le 2.0 \qquad (2.39)$$

where, $M = 2WaL$

$$d_{ij} = \frac{i^2}{2a} \left[2a(1-a) + \frac{1}{\pi^2 i^2} \left\{ 1 - \frac{\cos 2\pi ia + \cos 2\pi i(1-a)}{2} \right\} \right]; \quad i=$$

$$= \frac{i^2}{a\pi^2} \left[\frac{1-\cos (i+j)\pi a - \cos (i+j)\pi (1-a) + \cos (i+j)\pi}{(i+j)^2} \right.$$

$$\left. - \frac{1-\cos (i-j)\pi a - \cos (i-j)\pi (1-a) + \cos (i-j)\pi}{(i-j)^2} \right]; i \neq j$$

where, $i = 1, \ldots, n; \quad j = 1, \ldots, \bar{n}.$ (2.40)

$$h_{ij} = ij \frac{(-3.6 \bar{K} (2\rho - 1))}{\pi} \left[\int_0^{2a} (\alpha + (1-\alpha)\bar{z}) \frac{\bar{z}}{2a} \right.$$

$$\cos\frac{\pi i\bar{z}}{2}\cos\frac{\pi j\bar{z}}{2}\,d\bar{z} + \int_{2a}^{1}(\alpha+(1-\alpha)\bar{z})\cos\frac{\pi i\bar{z}}{2}\cos\frac{\pi j\bar{z}}{2}\,d\bar{z}$$

$$+\int_{1}^{2(1-a)}(2-\alpha-(1-\alpha)\bar{z})\cos\frac{\pi i\bar{z}}{2}\cos\frac{\pi j\bar{z}}{2}\,d\bar{z} + \int_{2(1-a)}^{2}(2-\alpha-(1-\alpha)\bar{z})$$

$$\frac{(2-\bar{z})}{2a}\cos\frac{\pi i\bar{z}}{2}\cos\frac{\pi j\bar{z}}{2}\,d\bar{z}\Big) - \frac{8\bar{K}}{\pi^3 a}\left(\frac{\bar{a}_{zi}}{h_{zi}}\right)\Big\{(\alpha+2a(1-\alpha))$$

$$\sin\pi ia\sin\pi ja + \{2-\alpha-2(1-a)(1-\alpha)\}\sin\pi i(1-a)\sin\pi j(1-a)$$

where, $i = 1, \ldots, \bar{n}$; $j = 1, \ldots, \bar{n}$. (2.41)

A computer program is developed to formulate the matrix [A] and the matrix [B]. Numerical integration scheme is adopted for evaluating h_{ij} and f_{ij} elements of the matrices. NAG Subroutine F02bjf is used to solve the eigenvalue problem of the form

$$[\,A\,]\{\,X\,\} = k\,[\,B\,]\{\,X\,\}.$$

The results of the analysis are presented and discussed in the next chapter.

CHAPTER III

RESULTS AND DISCUSSIONS

3.1 INTRODUCTION

In Chapter II, expressions for elements of the load matrix and the stiffness matrix were derived for various load cases. As seen from Eq. (2.27), the expression for f_i elements involves B_t, B_b, T_t, T_b, h and some combinations of these parameters. It is more convenient to use the clear height of web h_w, instead of h which is the distance between the flange centroids. Using h_w, the web/flange area ratio η at the centre can be written as

$$\eta = \frac{\mu\ (T_w/h_w)}{(B_t/h_w)\ (T_t/h_w)} = \frac{(1-\mu)\ (T_w/h_w)}{(B_b/h_w)\ (T_b/h_w)} \qquad (3.1)$$

If μ, ρ, (T_w/h_w), (B/h_w). (T/h_w) are known, then the section dimensions can be uniquely determined for a given h_w. Here B and T are the width and the thickness of the governing flange, i.e. the flange having higher moment of inertia about the minor axis of the member. (Top flange for $\rho > 0.5$ and bottom flange for $\rho<0.5$). For $\rho = 0.5$, flange having greater area will be the governing flange.

In general, the stability condition for beam-columns / tie-beams should be influenced by the parameters ρ, μ, $\bar{K}$, α and (T_w/h_w), (B/h_w), (T/h_w). However, in practice the range of variation in the values of last three parameters is very small. For example, for ISMB sections the value of μ is 0.5; (T_w/h_w) is

in the range 0.022 to 0.032; (B/h_w) varies from 0.38 to 0.56 and (T/h_w) varies from 0.04 to 0.06. Therefore, it will be justified if we keep μ, (T_w/h_w), (B/h_w), (T/h_w) constant and study the flexural-torsional buckling for various combinations of ρ, α, $\bar{K}$ and k only. For the purpose of present analysis, following values are adopted:

$$\mu = 0.5,\ (T_w/h_w) = 0.025,\ (B/h_w) = 0.467,\ (T/h_w) = 0.04.$$

Beam-columns/tie-beams with α = 0.25, 0.50, 0.75, 1.0 and ρ = 0.1, 0.3, 0.5, 0.7, 0.9 have been studied for various load combinations with axial load ratio varying from -1.0 to +1.0. The value of the parameter $\bar{K}$ varies from 0.0 to 2.0.

Convergence studies were conducted to determine the number of terms in the trigonometric series (Eq. 2.20) required for accurate solutions. It was found that for prismatic members with syymmetric loads, $n = \bar{n} = 3$ terms are sufficient. However, for tapering members and unsymmetric loading, atleast 7 terms are required. The numerical results presented herein are based on $n = \bar{n} = 7$.

3.2 MOMENT GRADIENT LOADING CASE

A typical stability criteria curve for monosymmetric, prismatic beam-columns with $\rho > 0.5$ and subjected to uniform sagging moment is shown in Fig. 3.1. The point A corresponds to flexural-torsional buckling load for columns. If the combination of λ and k is such that it falls inside the area enclosed by the curve, the member is stable. When the axial load ratio exceeds the value λ_0, member is unstable unless accompanied by adequate applied moment within the stability criterion (i.e. between points B and C in Fig. 3.1). The applied moment serves to stabilize the

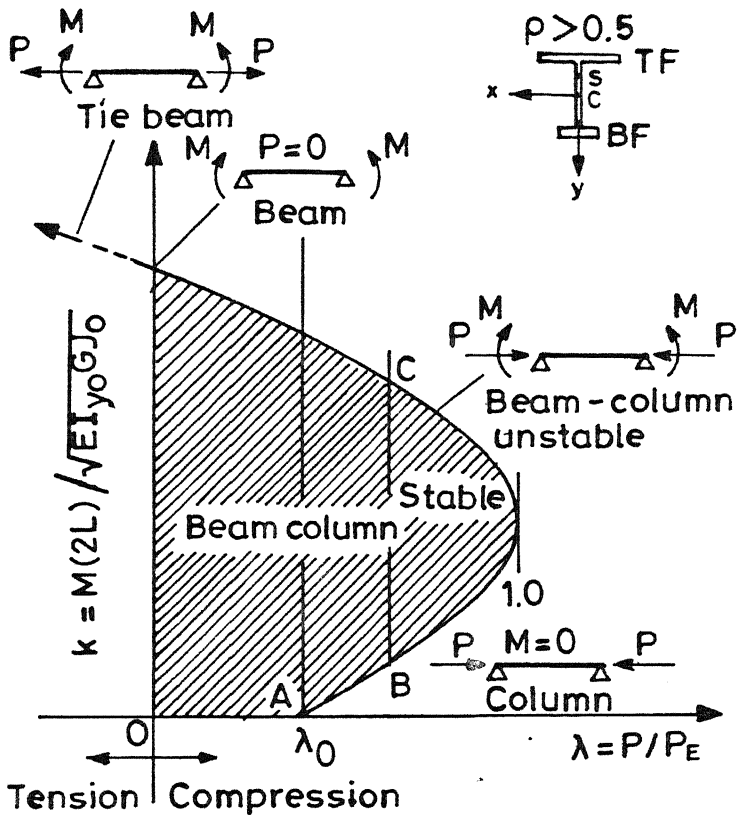

Fig. 3.1 Typical stability criteria curve for monosymmetric beam-columns.

member by decreasing the compressive normal stresses in the smaller flange which is further away from the shear centre; thereby decreasing the destabilizing torque caused by the compressive stress components as the section warps during buckling (This is the Wagner effect). For stability, the applied moment must be sufficiently large such that the resulting stresses in the smaller flange become tensile so as to provide an effective restoring torque (Fig. 3.2). On the other hand, when the applied moment is too large, the member will become unstable because the larger flange is not able to sustain the increased compressive stresses (above point C in Fig. 3.1). The same explanation is valid for prismatic beam-columns with $\rho < 0.5$ and subjected to uniform hogging moment. Results for moment gradient loading are presented in Figs. 3.3 to 3.10.

Figures 3.3 to 3.6 give stability criteria for a typical monosymmetric tapering member with $\bar{K} = 1.0$, $\alpha = 0.25$, 1.0 and $\rho = 0.1$, 0.5, 0.9: values of β considered are -1.0, 0.0 and 0.5; axial load λ varies from -1.0 to +1.0. Figures 3.7 - 3.9 show influence of α and ρ on the buckling capacity for $\bar{K} = 1.0$, $\lambda = -1.0$, 0.0, 0.5 and $\beta = -1.0$, 0.0, +1.0. The Fig. 3.10 shows influence of $\bar{K}$ and ρ on buckling capacity for $\alpha = 0.25$, 1.0, $\lambda = 0.25$, 0.75 and for $\beta = 0.5$. From these results following points can be noted:

(i) For single curvature bending of prismatic members (Figs. 3.3a and 3.4a), the buckling capacity k increases with increasing ρ value for the sagging moment case, while for the hogging moment k increases with decreasing ρ value. This may be attributed to the Wagner effect which is more favourable when the flange with the smaller I_y is in tension during buckling (Kitipornchai and Wang, 1988b).

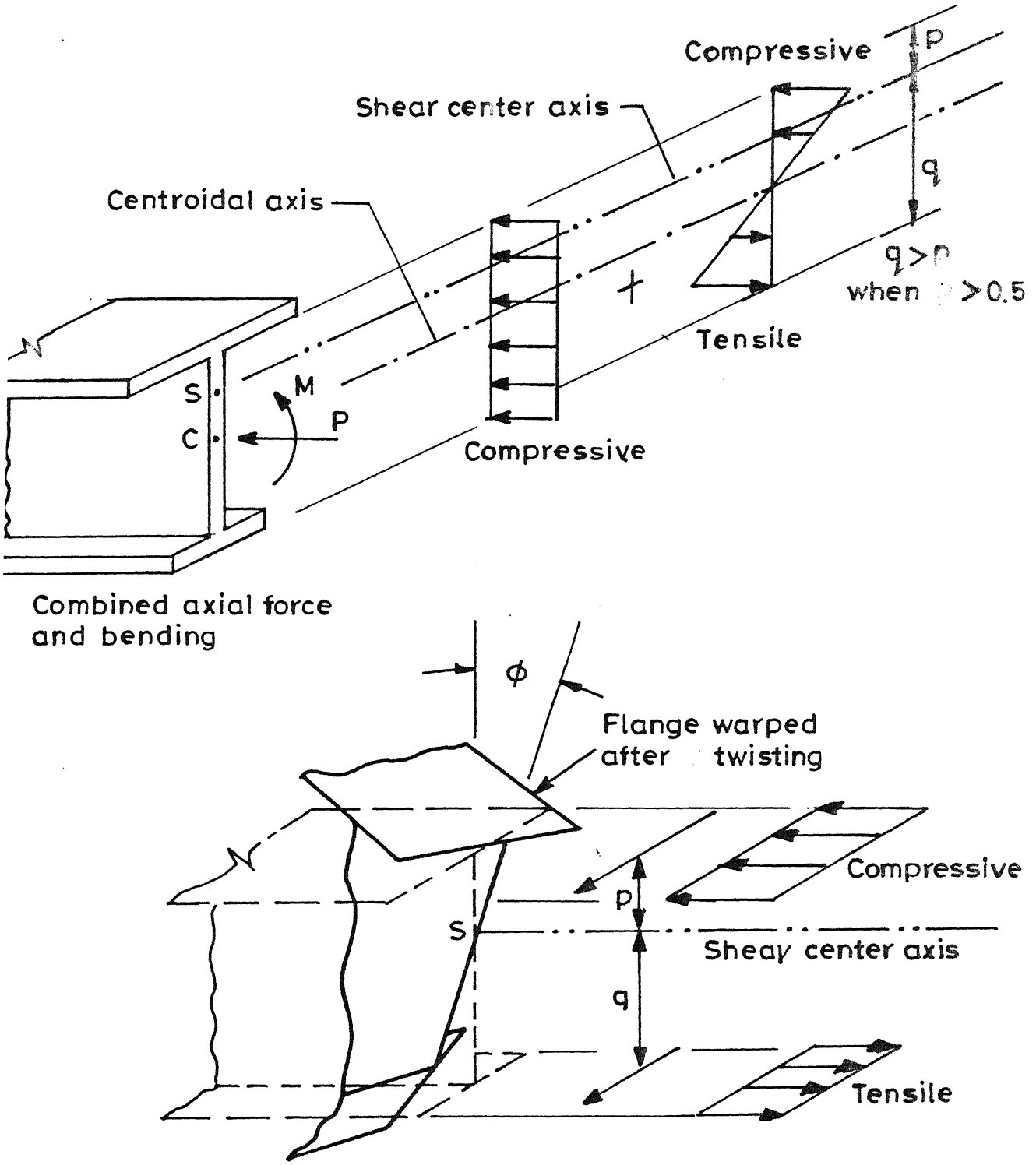

Fig. 3.2 Influence of tensile stresses in smaller flange.

(ii) The trend similar to that in (i) is observed for tapered members when the axial load is compressive (Figs. 3.3b and 3.4b); however, it is not so when the axial load is tensile and sufficiently large. the axial tension P causes the major axis moment Py_{oz}. This component acts in the same direction as the externally applied moment and therefore has a tendency to destabilize the member. When the axial tension is small this component is over shadowed by the Wagner effect, but it becomes significant when the axial tension is large. That is why the buckling curve for ρ = 0.5 is higher than that for ρ = 0.9, when axial tension is very large. The effect is even more severe for ρ = 0.1 and for hogging moment case, where in addition to Py_{oz}, Pe_z also acts in the direction of the externally applied moment.

(iii) For double curvature bending (β > 0), the Wagner effect has a mixed influence, since smaller flange at one end is in compression while at the other end it is in tension. Figs. 3.5a and 3.6a show that buckling capacity for prismatic member will be greatly curtailed if axial compression is very high. The buckling behaviour is governed by the portion of smaller flange which is under compression. As expected, for β = +1.0 the buckling capacity for ρ and $(1-\rho)$ is the same. The buckling capacity is greatest for doubly symmetric sections (Fig. 3.6a).

(iv) Figures 3.5b and 3.6b show stability criteria for tapered members under moment gradients with β = +0.5 and β = +1.0, respectively. For ρ = 0.1 and high axial compression, a significant reduction in the buckling capacity takes place. But it is not so for ρ = 0.9 because the component Pe_z of the

major axis moment reduces the portion of smaller flange which is subjected to compressive stresses. For β = +1.0 and with axial tension ($-1.0 \leq \lambda \leq 0$), the buckling capacity for ρ and $(1-\rho)$ is almost the same.

(v) Figure 3.7 shows behaviour of tapering beam (λ = 0) under moment gradient case. For single curvature bending ($\beta \leq 0$), as the value of α increases, the buckling capacity reduces for high values of ρ. This is again due to Wagner effect. For $\rho < 0.5$, the smaller flange is under compression which has a tendency to destabilize the member by reducing effective torsional rigidity. As the value of α increases, the distance of smaller flange from the shear centre increases which further increases the destabilizing torque. Thus buckling capacity reduces with increasing α. Just the reverse is the case when $\rho > 0.5$.

(vi) For double curvature bending of beams (β = +1.0, Fig. 3.7), the buckling capacity for ρ and $(1-\rho)$ is equal and is highest for a symmetric section. It is interesting to note that for extreme values of ρ, the Wagner effect is more prominent. As the section monosymmetry reduces (ρ approaches 0.5), Wagner effect diminishes.

(vii) For single curvature bending of beam-columns ($\beta \leq 0$, Fig. 3.8), the buckling capacity decreases with decreasing α for all values of ρ. for $\rho < 0.5$, Py_{oz} and Pe_z components of the major axis moment acts in the same direction as the externally applied moment. As α decreases, Pe_z component increases, which increases the effective moment at the centre

of the member. Thus buckling capacity decreases. For $\rho > 0.5$, Py_{oz} component of major axis moment reduces the eternally applied moment. As α decreases, the effective moment near the end of the member (where cross section is least) increases. Thus the buckling capacity reduces.

(viii) The behaviour of beam-columns under double curvature bending ($\beta = +1.0$ Fig. 3.8) is similar to the single curvature bending case, when $\rho < 0.5$, i.e. the buckling capacity decreases with decreasing α. But for $\rho > 0.5$, the buckling capacity reduces with increasing value of α. The Pe_z component of major axis moment reduces the portion of the smaller flange which is under compression. As α increases, Pe_z decreases, thus increasing the portion of the smaller flange under compressive stresses. This results in reduction in the buckling capacity.

(ix) Figure 3.9 shows the behaviour of tie-beams under moment gradient. For single curvature bending ($\beta \leq 0$), the behaviour is similar to the beam case (Fig. 3.7, $\beta \leq 0$) except for very low value of α, where the buckling capacity for $\rho > 0.5$ reduces with increasing ρ value. The reason is that, for $\rho > 0.5$, Py_{oz} component increases the effective moment and for low values of α it over shadows the Wagner effect.

(x) For double curvature bending of tie-beams ($\beta = +1.0$, Fig. 3.9), a doubly symmetric section has the highest buckling resistance. For all values of ρ, the buckling capacity increases with increasing α.

(xi) Figure 3.10 shows the influence of $\bar{K}$ on buckling capacity. It is interesting to note that for prismatic member ($\alpha = 1.0$,

Fig. 3.10a), with very high value of ρ and with large axial compression, virtually there is no buckling resistance for $\bar{K}$ > 1.0. However, it is not so for the case of tapered member with α = 0.25. As mentioned earlier (Refer Fig. 3.5b, sagging moment case), this is because of the presence of Pe_z, which reduces the portion of smaller flange under compression.

3.3 TRANSVERSE LOAD CASES

Results for transverse load cases are presented in Figs. 3.11 - 3.15. the stability criteria for tapering monosymmetric members under central point load (assumed at shear centre) is given in Fig. 3.11 for $\bar{K}$ = 1.0, α = 0.25, 1.0 and ρ = 0.1, 0.5, 0.9. Figure 3.12 shows the influence of α and ρ on the buckling capacity with $\bar{K}$ = 1.0 and λ = −1.0, 0.0, 0.5. The influence of load height below the shear centre for $\bar{K}$ = 1.0, α = 0.25, 1.0 and ρ = 0.5 is shown in Fig. 3.13. the effect of the positioning of the single point load along the span can be seen in Fig. 3.14 for ρ = 0.1, 0.5, 0.9; λ = −1.0, 0.0, 0.5; $\bar{K}$ = 1.0 and α = 1.0. Similar effect in the case of two point loads is shown in Fig. 3.15. From these results following points can be noted:

(i) It is seen from Fig. 3.11 that for λ > 0.25, the buckling curves are similar to those in Fig. 3.3 for the uniform sagging moment case, that is, k increases with decreasing λ and with increasing ρ values. However, when the axial load is tensile (λ < 0), the buckling capacity for ρ = 0.9 is less than that for ρ = 0.1 and ρ = 0.5. (This is because of Py_{oz} component which acts in the same direction as the external moment when ρ > 0.5. This component increases the effective

moment, over shadows the Wagner effect and thus reduces the buckling capacity.) A similar trend in the results is observed when transverse load is in the form of a uniformly distributed load and two point loads.

(ii) For beams (λ = 0.0) the value of k increases with increasing value of ρ, except for ρ = 0.9 where the buckling capacity reduces considerably (Fig. 3.12b). Similar result has also been reported earlier for prismatic monosymmetric member under central point load. The reason is, that for very high value of ρ (T - section), the buckled mode shape for angle of twist $\bar{\phi}$, changes to more complex lower buckled mode shape (Wang and Kitipornchai, 1986b). For beam columns (λ = 0.50, Fig. 3.12c), the behaviour is similar to that for the uniform sagging moment case (β = -1.0, Fig. 3.8). For tie-beams (λ = -1.0, Fig. 3.12a), the buckling capacity reduces considerably for $\rho \geq 0.5$. This is because of predominant effect of Py_{oz}. A similar trend in the results is observed when the transverse load is in the form of a uniformly distributed load and two point loads.

(iii) It is clear from Fig. 3.13 that the buckling load increases as the point of application of the load moves towards the bottom flange. The bottom flange loading causes a stabilizing torque as the twisting of the cross-section occurs during buckling; the top flange loading causes a torque which further destabilizes the member. Thus, the buckling capacity for bottom flange loading is higher than that for shear centre loading and it is least for top flange loading. The behaviour is found to be similar for other values of ρ as well.

(iv) Figure 3.14 shows that for $\rho > 0.5$, the buckling capacity of a member reduces as the point load moves towards the mid span. No significant change in buckling capacity is observed for low values of ρ. The behaviour is found to be similar for other values of α as well.

(v) In case of two point loads and $\rho < 0.5$ (Fig. 3.15), the buckling capacity of a member increases as the distance between the loads decreases (i.e. as the value of a increases). For $\rho > 0.5$ however, the buckling capacity first reduces and then increases. The behaviour is found to be similar for other values of α as well.

3.4 COMPARISON WITH IS SPECIFICATIONS

IS:800 (1984) proposes the following formula for determining elastic critical stress f_{cb} (in MPa):

$$f_{cb} = \frac{26.5 \times 10^5}{(l/ry)^2} \left[K_2 + \left\{ 1 + \frac{1}{20} \left(\frac{l}{r_y} \frac{T}{D} \right)^2 \right\}^{1/2} \right] \frac{C_2}{C_1} \qquad (3.2)$$

where,

l = effective length of compression flange;

r_y = radius of gyration of the section about its axis of minimum strength;

T = mean thickness of the compression flange;

D = overall depth of beam;

C_1, C_2 = respectively the lesser and greater distances from the section neutral axis to the extreme fibre;

K_2 = a coefficient to allow for the inequality of flanges, and depends on ω, the ratio of the moment of inertia of the compression flange alone to that of the sum of moments of inertia of the flanges,

each calculated about its own axis parallel to the Y-Y axis of the girder, at the point of maximum bending moment. Value of K_2 is given by;

$K_2 = 0.5\ (2\omega - 1)$ for $\omega > 0.5$

$= 2\omega - 1$ for $\omega \leq 0.5$

The above code provisions do not take into account the effect of web tapering, the loading condition, load height below shear centre, the nature of axial force etc. The values of f_{cb} calculated as per the code provisions are compared with those obtained from present analysis; this comparision is given in Tables 3.1 and 3.2 for prismatic beams ($\alpha = 1.0$, $\lambda = 0.0$). The details of sections used are listed below:

No.	ρ	h_w (mm)	B_t (mm)	T_t (mm)	B_b (mm)	T_b (mm)	T_w (mm)
1.	0.1	300.0	46.0	38.0	140.0	12.5	7.5
2.	0.3	300.0	92.0	19.0	140.0	12.5	7.5
3.	0.5	300.0	140.0	12.5	140.0	12.5	7.5
4.	0.7	300.0	140.0	12.5	92.0	19.0	7.5
5.	0.9	300.0	140.0	12.5	46.0	38.0	7.5

Note that for all the sections considered $\mu = 0.5$, $(B/h_w) = 0.467$, $(T/h_w) = 0.04$ and $(T_w/h_w) = 0.025$.

Table 3.1 compares f_{cb} for prismatic, monosymmetric beams under uniform sagging moment load case (moment gradient with $\beta = -1.0$, ρ varying from 0.1 to 0.9; l/ry varying from 100 to 300). Table 3.2 shows the comparison for prismatic doubly symmetric

beams under various loading cases. A study of above tables reveal following important points:

(i) For $\rho \leq 0.5$, IS code provisions give unsafe value of f_{cb}. It over estimates f_{cb} by 46% to 50% for $\rho = 0.1$, and 15% to 18% for $\rho = 0.5$, depending on the slenderness ratio.

(ii) For $\rho > 0.5$, IS:800 gives conservative values of f_{cb}. For $\rho = 0.9$ it under estimates f_{cb} by 27% to 40%.

(iii) For doubly symmetric beams with transverse loads placed on the top flange, the value of f_{cb} obtained as per code specifications is unsafe.

For the central point load case, Eq. (3.2) over estimates f_{cb} by 8% to 29%; for the uniformly distributed load case the error is 24% to 44%.

(iv) For doubly symmetric beams with transverse loads placed on bottom flange, IS:800 gives conservative values of f_{cb}.

For the central point load case, IS:800 under estimates f_{cb} by 30% to 45%, while for the uniformly distributed load case the error is 12% to 28%.

Tables 3.3 to 3.10 give values of non dimensional buckling capacity k, for doubly symmetric sections under various loading cases. The value of α is either 0.5 or 1.0. The axial load ratio varies from −1.0 to +1.0, while $\bar{K}$ varies from 0.25 to 2.0. Once a value of k is picked up from the appropriate table, the f_{cb} can be obtained as

$$f_{cb} = \frac{M}{Z_{x\ min}} = \frac{k\sqrt{EI_{yo}GJ_o}}{(2L)\ I_x} C_2 \qquad (3.3)$$

3.5 SCOPE OF FURTHER RESEARCH

The present investigation is based on certain simplifying assumptions, which are listed in Sec. 2.1. Further improvement is possible along the following lines:

(i) The buckling capacity of a member may be increased by the proper use of a system of lateral bracing. Such systems may consist of either discrete braces (e.g. series of cross beams connected to the member) or of a continuous lateral restraint (e.g. members supporting concrete floor). Most bracing arrangements in an I section member can be represented by an idealized spring system consisting of an elastic lateral brace at a certain distance above the shear centre of the cross section and an elastic rotational brace at shear centre. Flexural-torsional behaviour can be investigated for such bracings placed at various positions along the span.

(ii) End restraints assumed in the present analysis are:

- No lateral displacement and moment at supports.
- Zero twist and zero warping restraint at supports.

Similar investigation can be carried out for other boundary conditions also.

(iii) The analysis deals with two way tapering members which are used essentially for plate girders or gantry girders. Sometimes, one way tapering members are used in frame construction (e.g. legs of a hinged portal or gable frame). The flexural-torsional behaviour of such members can be investigated for various types of end restraints.

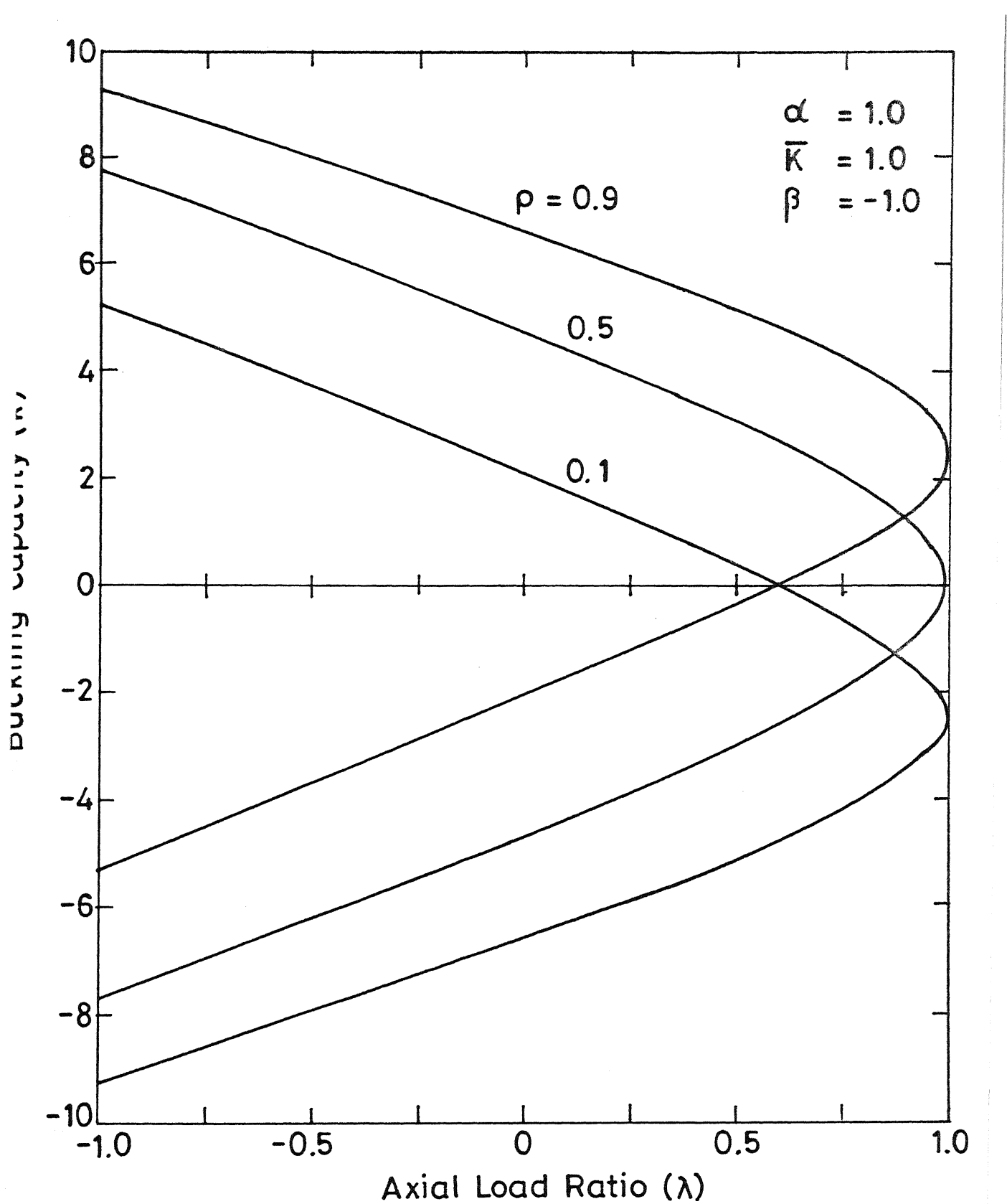

Fig. 3.3(a) Stability criteria for monosymmetric beam-column tie-beams under uniform moment, $\beta = -1.0$, $\alpha = 1.0$

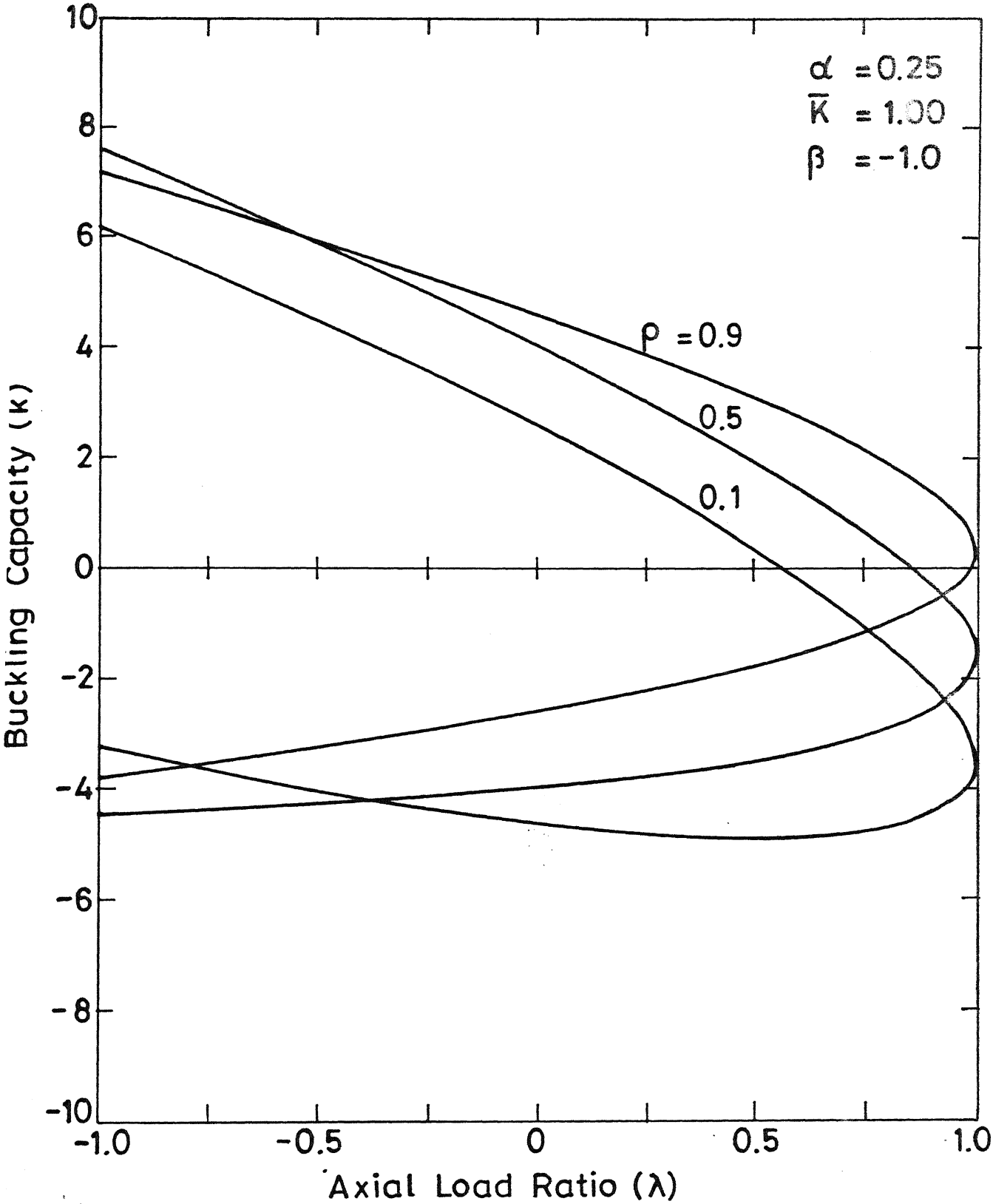

Fig.3.3(b) Stability criteria for monosymmetric beam-columns tie-beams under uniform moment ; $\beta = -1.0$, $\alpha = 0.25$

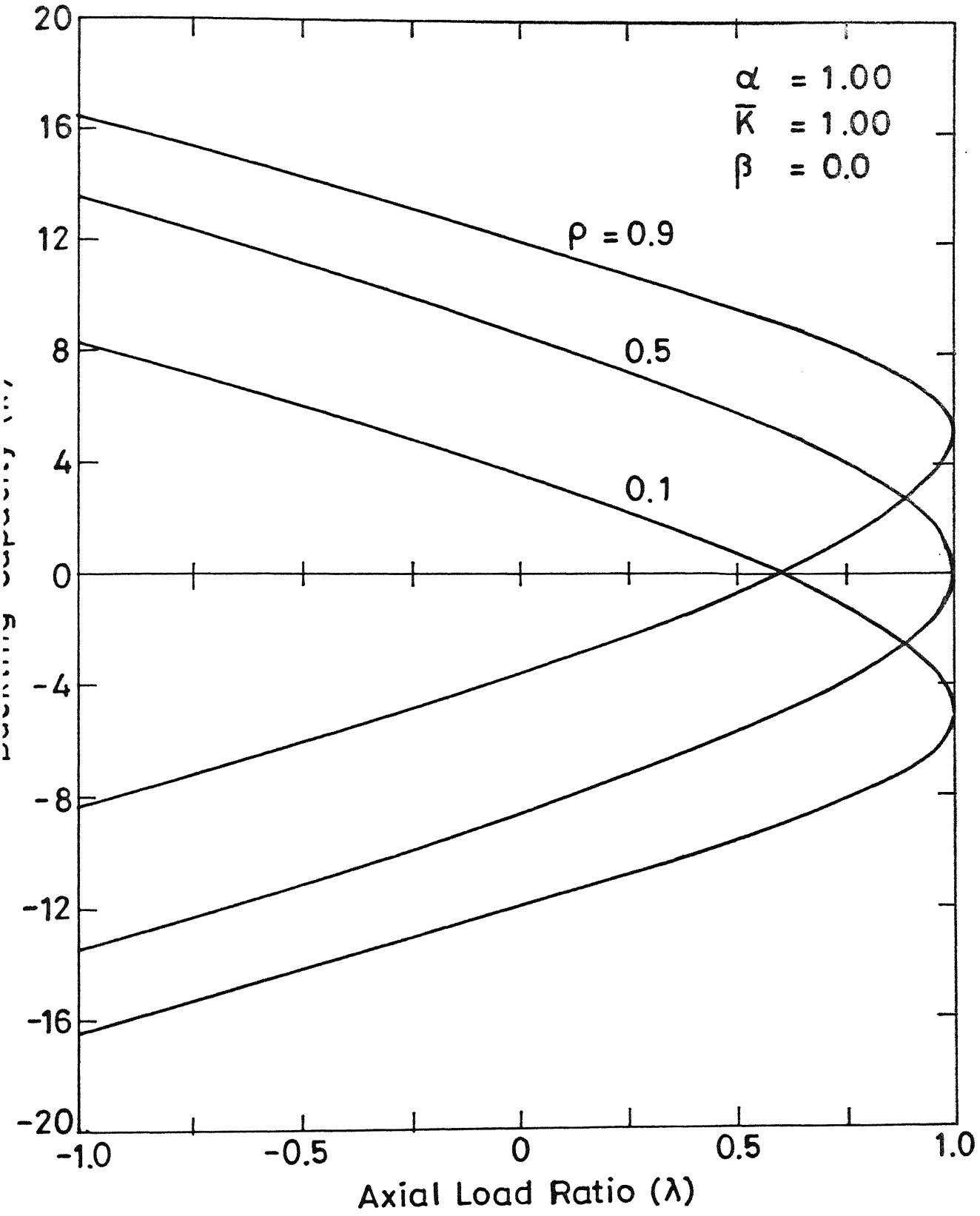

Fig. 3.4(a) Stability criteria for monosymmetric beam-columns / tie-beams under one end moment, $\beta = 0$, $\alpha = 1.0$.

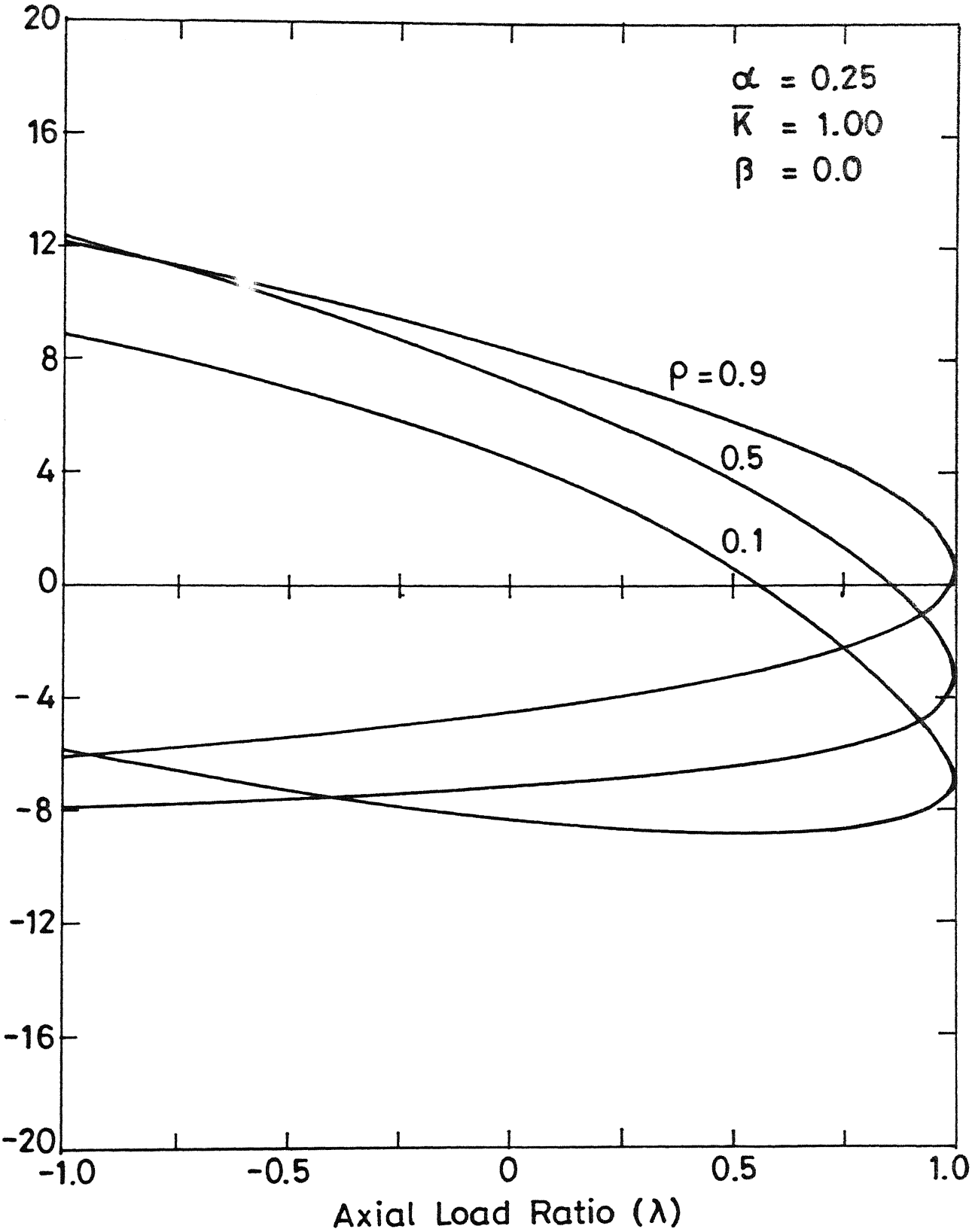

Fig.3.4(b) Stability criteria for monosymmetric beam-columns/ tie-beams under one end moment, $\beta = 0$, $\alpha = 0.25$.

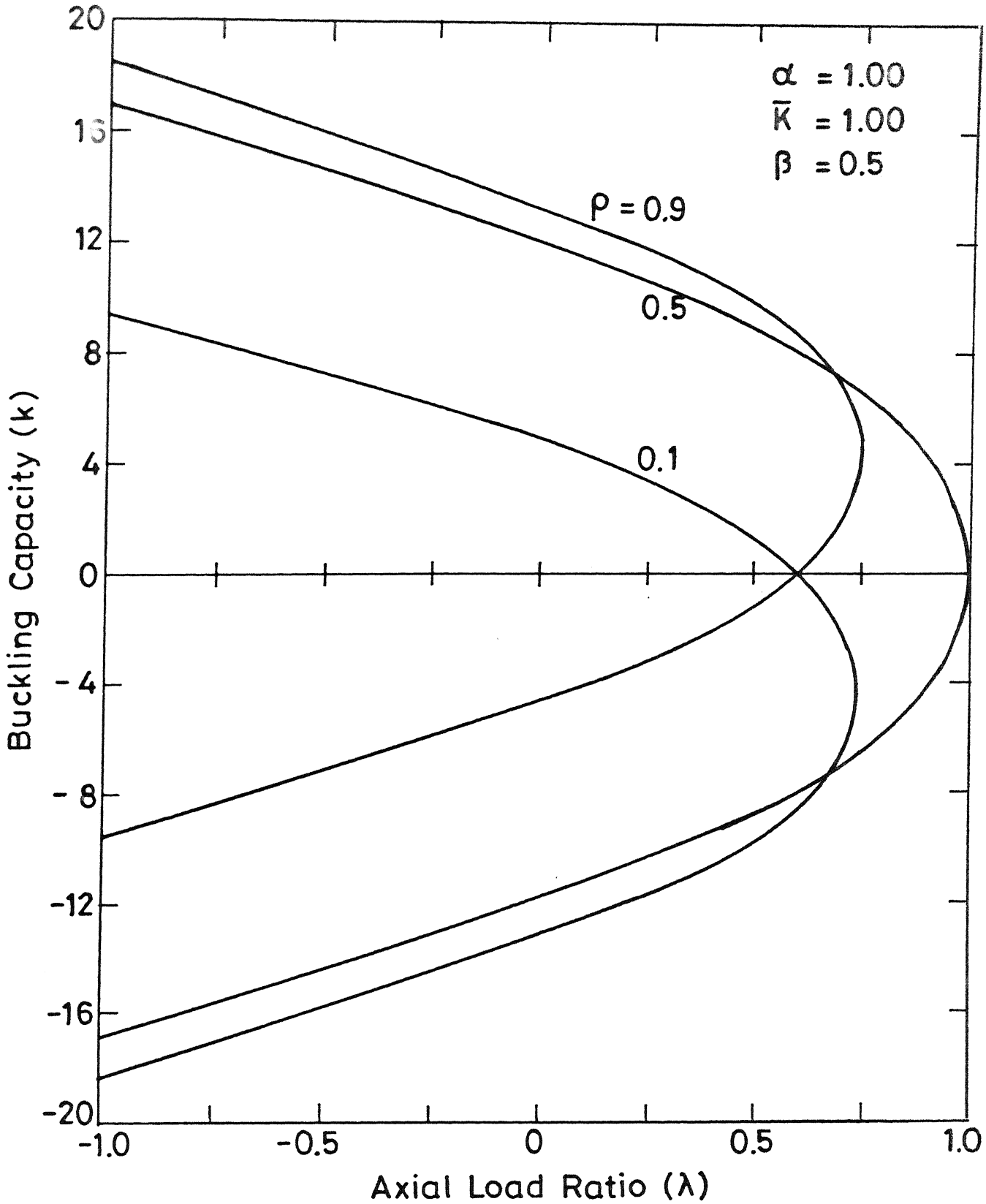

Fig. 3.5(a) Stability criteria for monosymmetric beam-column tie-beams under moment gradient, $\beta = 0.5$, $\alpha = 1.0$

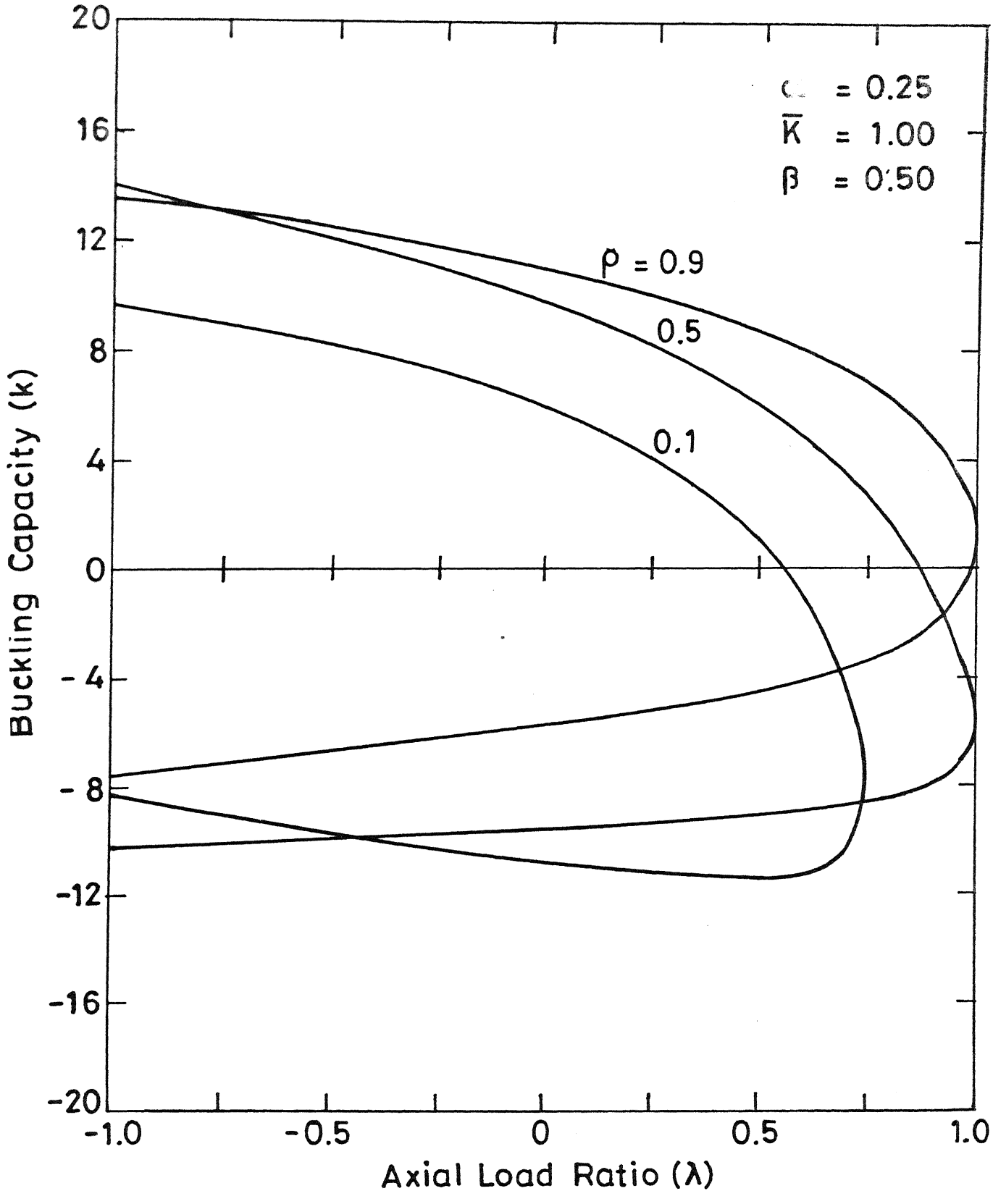

Fig. 3.5(b) Stability criteria for monosymmetric beam-columns tie-beams under moment gradient, $\beta = 0.5$, $\alpha = 0.2$

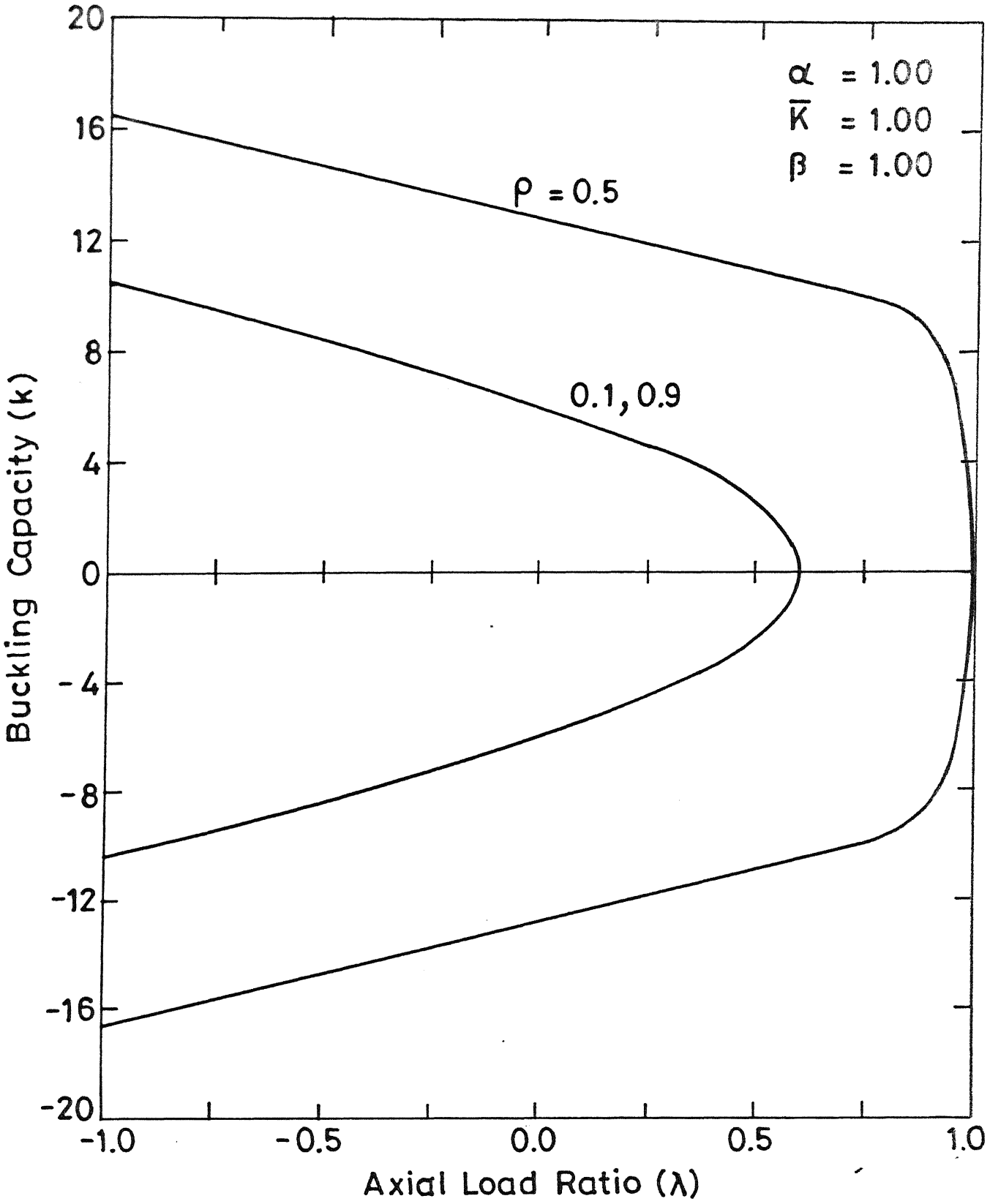

Fig. 3.6(a) Stability criteria for monosymmetric beam-column tie-beams under moment gradient, $\beta = 1.0$, $\alpha = 1.0$

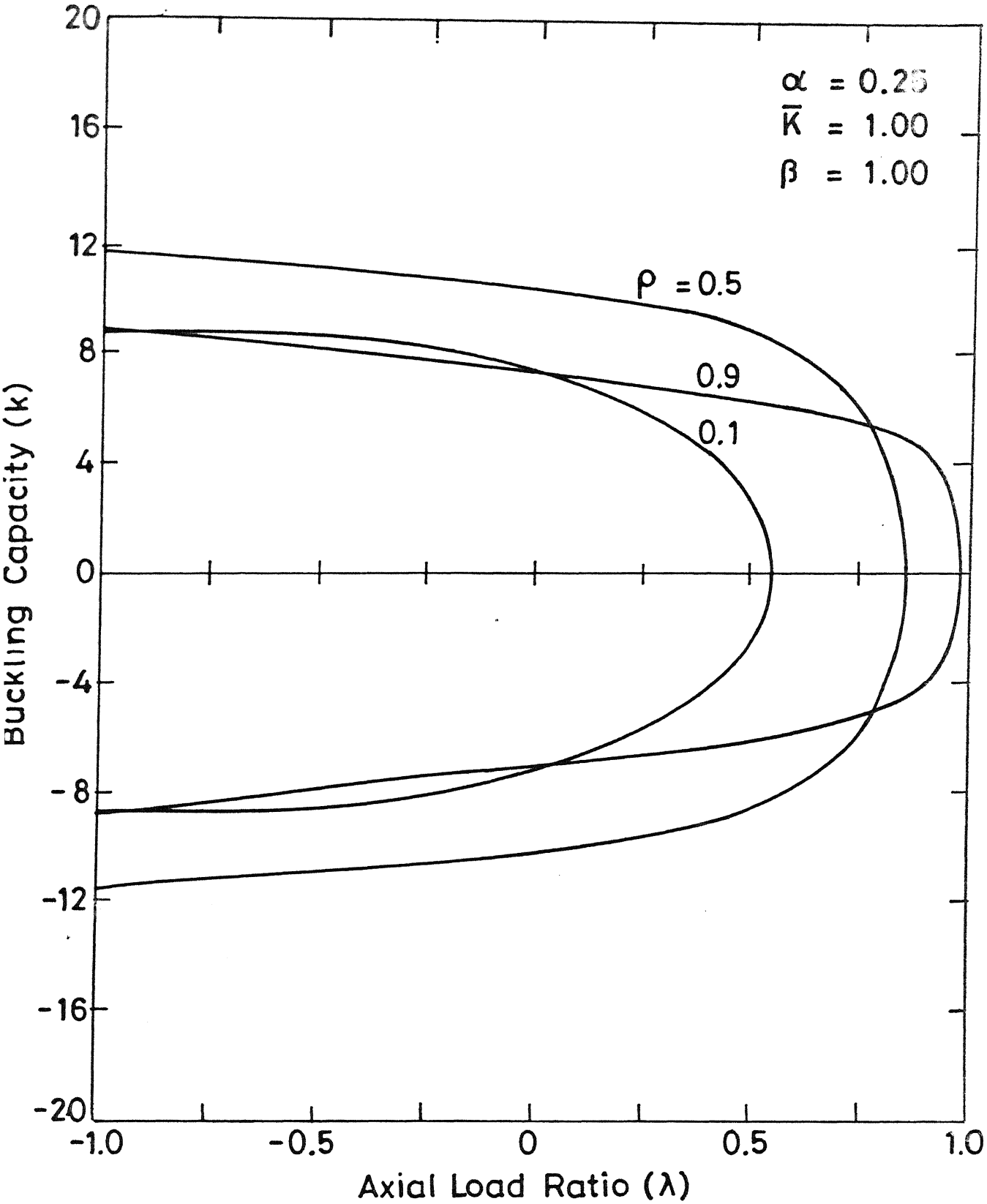

Fig. 3.6(b) Stability criteria for monosymmetric beam-columns tie-beams under moment gradient, $\beta = 1.0$, $\alpha = 0.25$

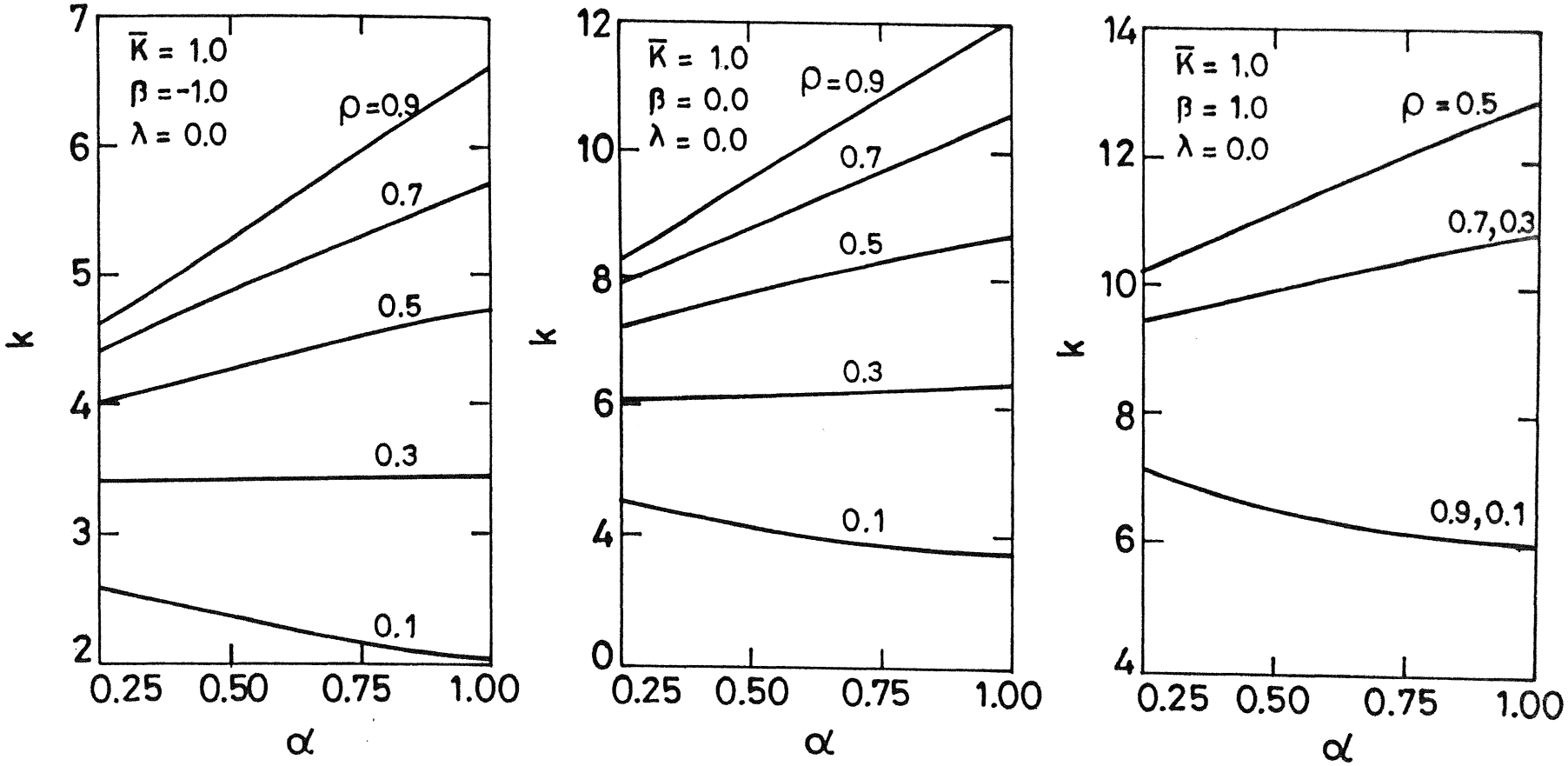

Fig.3.7 Influence of α and ρ on buckling capacity of beams (λ=0) under moment gradient.

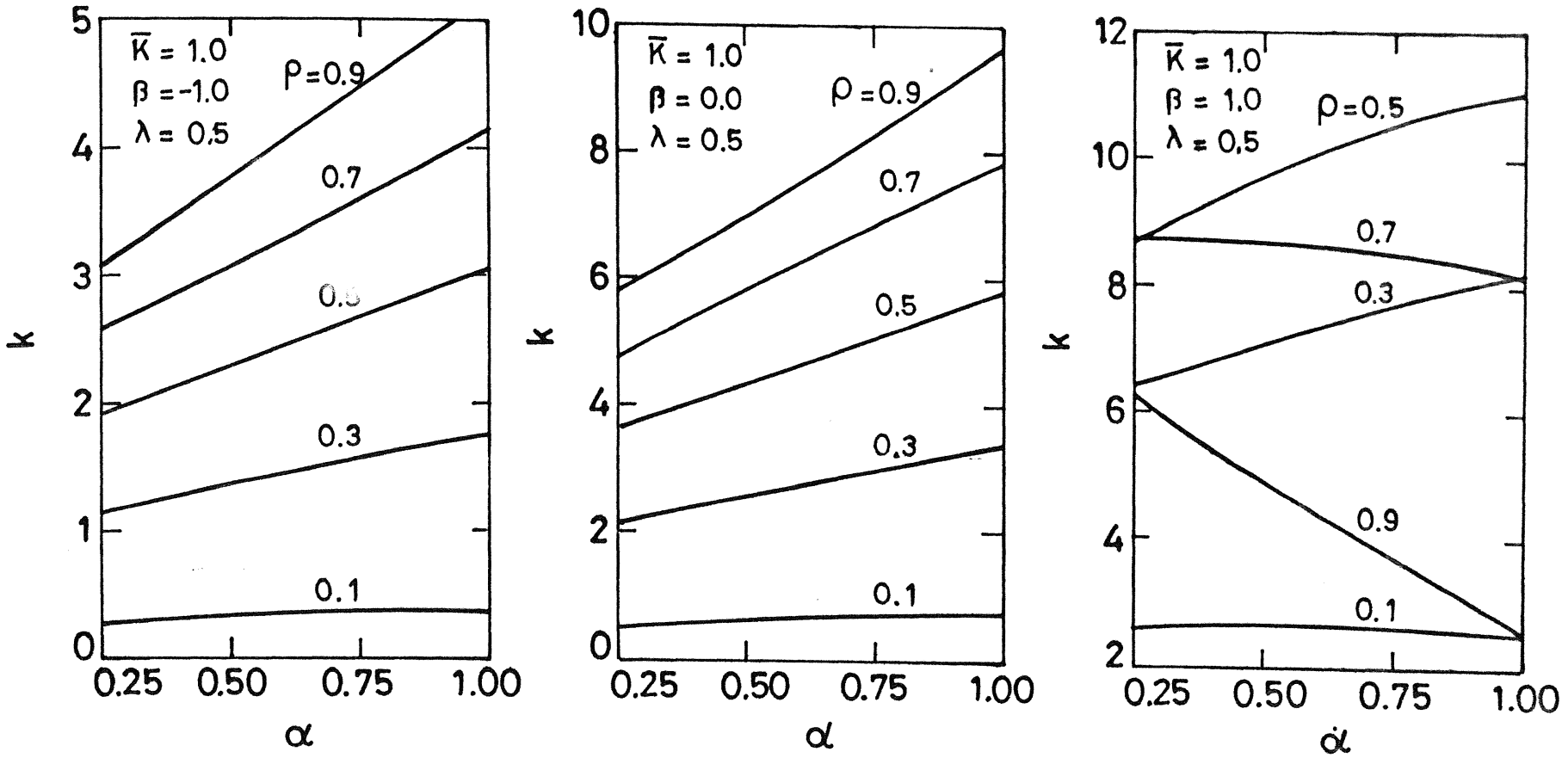

Fig. 3.8 Influence of α and ρ on buckling capacity of beam-columns (λ=0.5) under moment gradient.

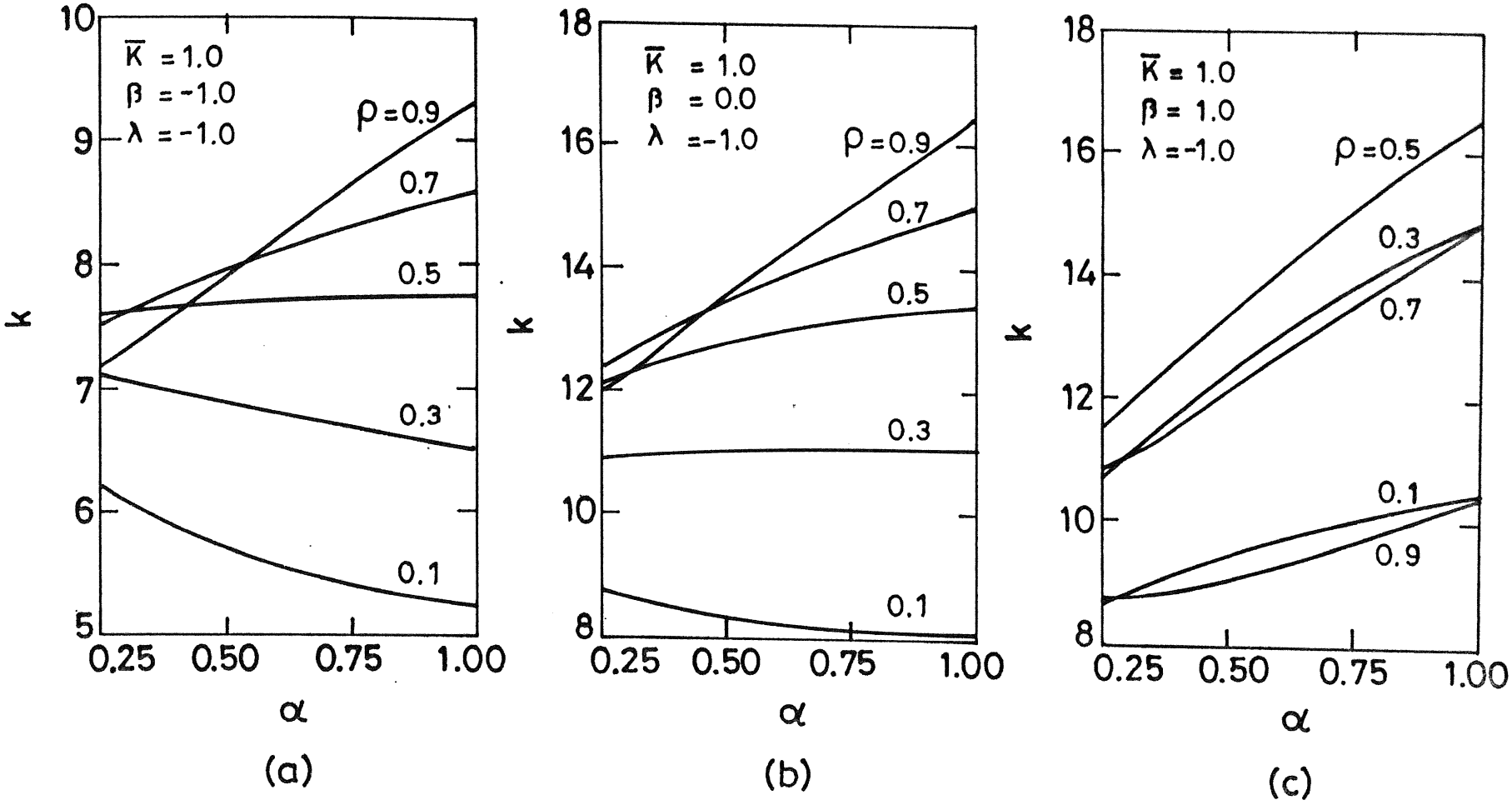

Fig. 3.9 Influence of α and ρ on buckling capacity of tie-beams (λ = -1.0) under moment gradient.

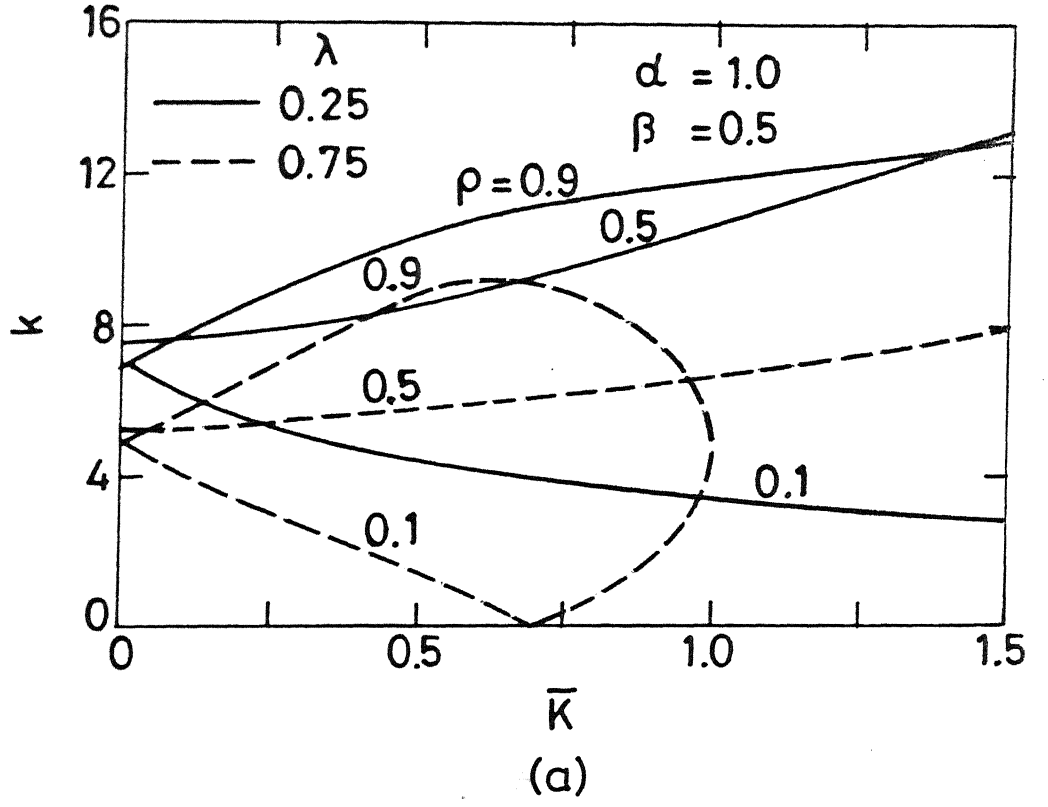

(a)

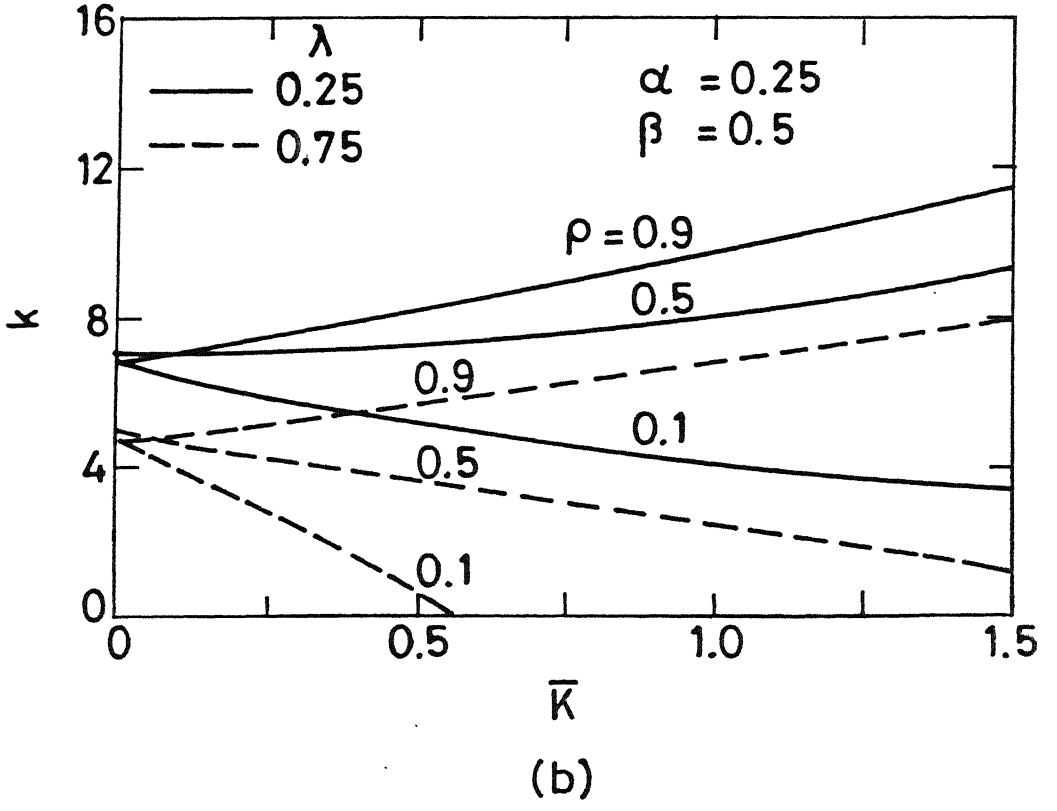

(b)

Fig.3.10 Influence of $\bar{K}$ on buckling capacity of monosymmetric beam-columns under moment gradient, $\beta = 0.50$

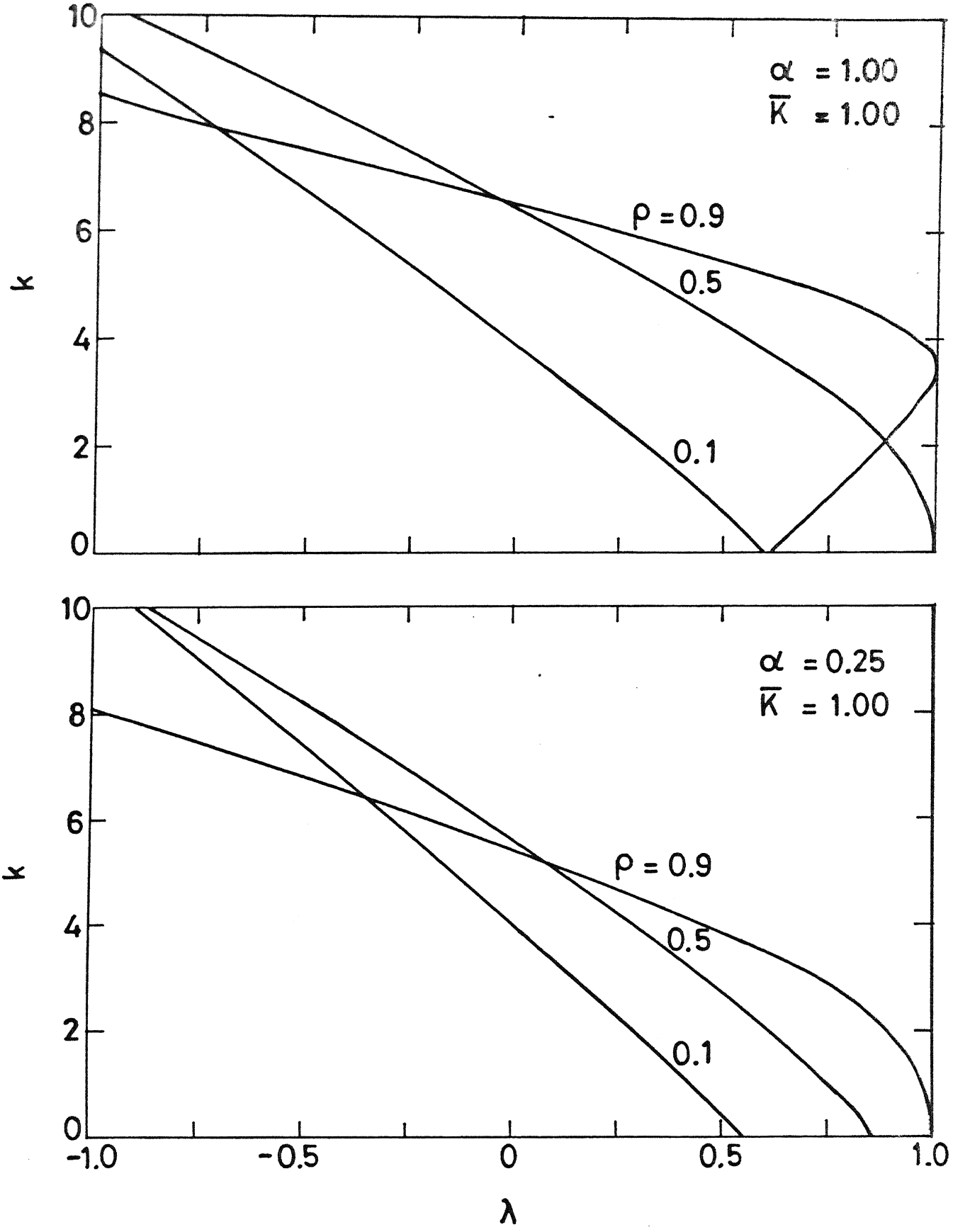

Fig. 3.11 Stability criteria for monosymmetric beam-columns / tie-beams under central point load (SC)

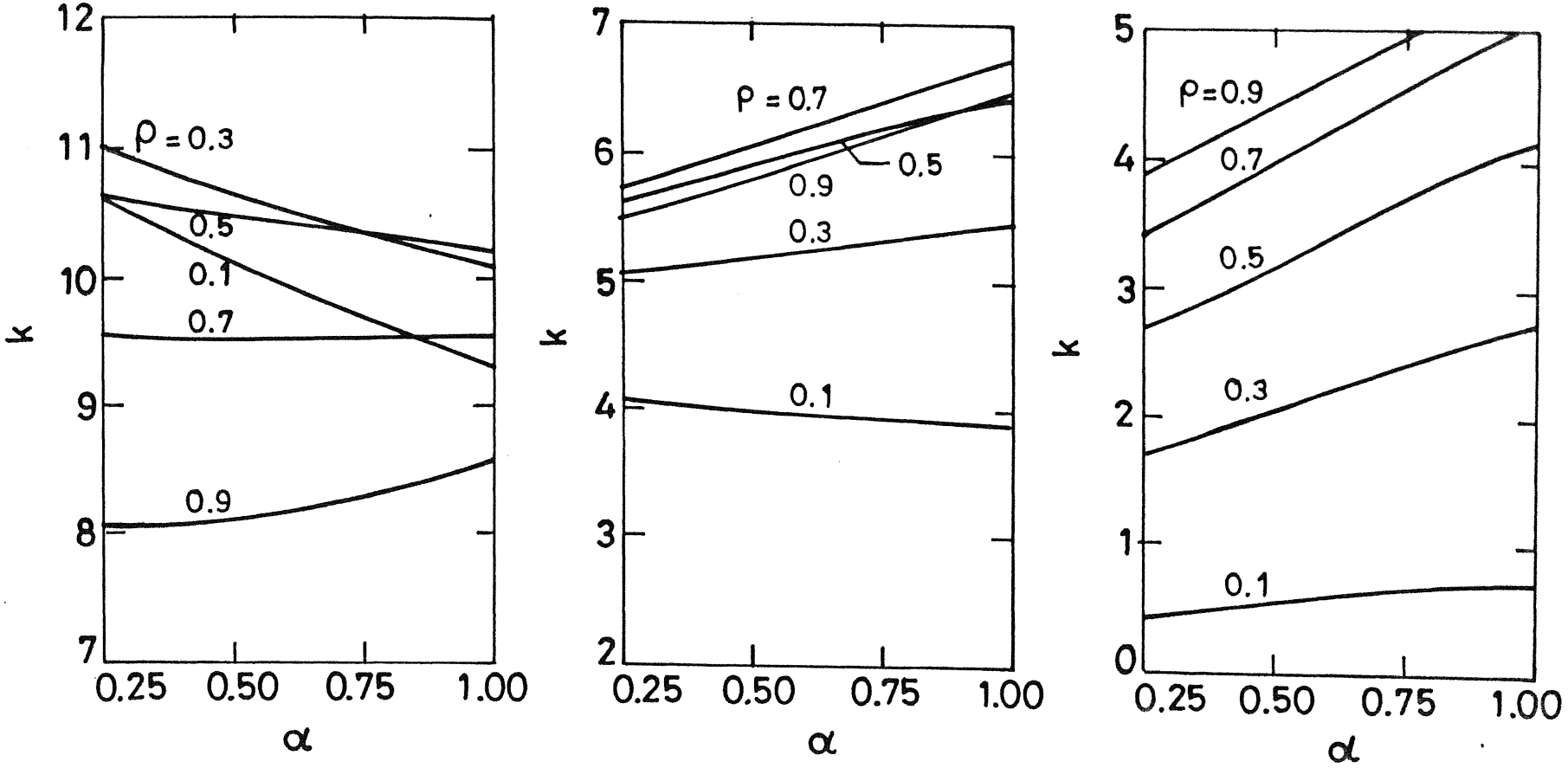

(a) Tie-beams ($\lambda = -1.0$, $\bar{K} = 1.0$)

(b) Beams ($\lambda = 0.0$, $\bar{K} = 1.0$)

(c) Beam-columns ($\lambda = 0.50$, $\bar{K} = 1.0$)

Fig, 3, 12 Influence of α and ρ on buckling capacity under central point load (SC).

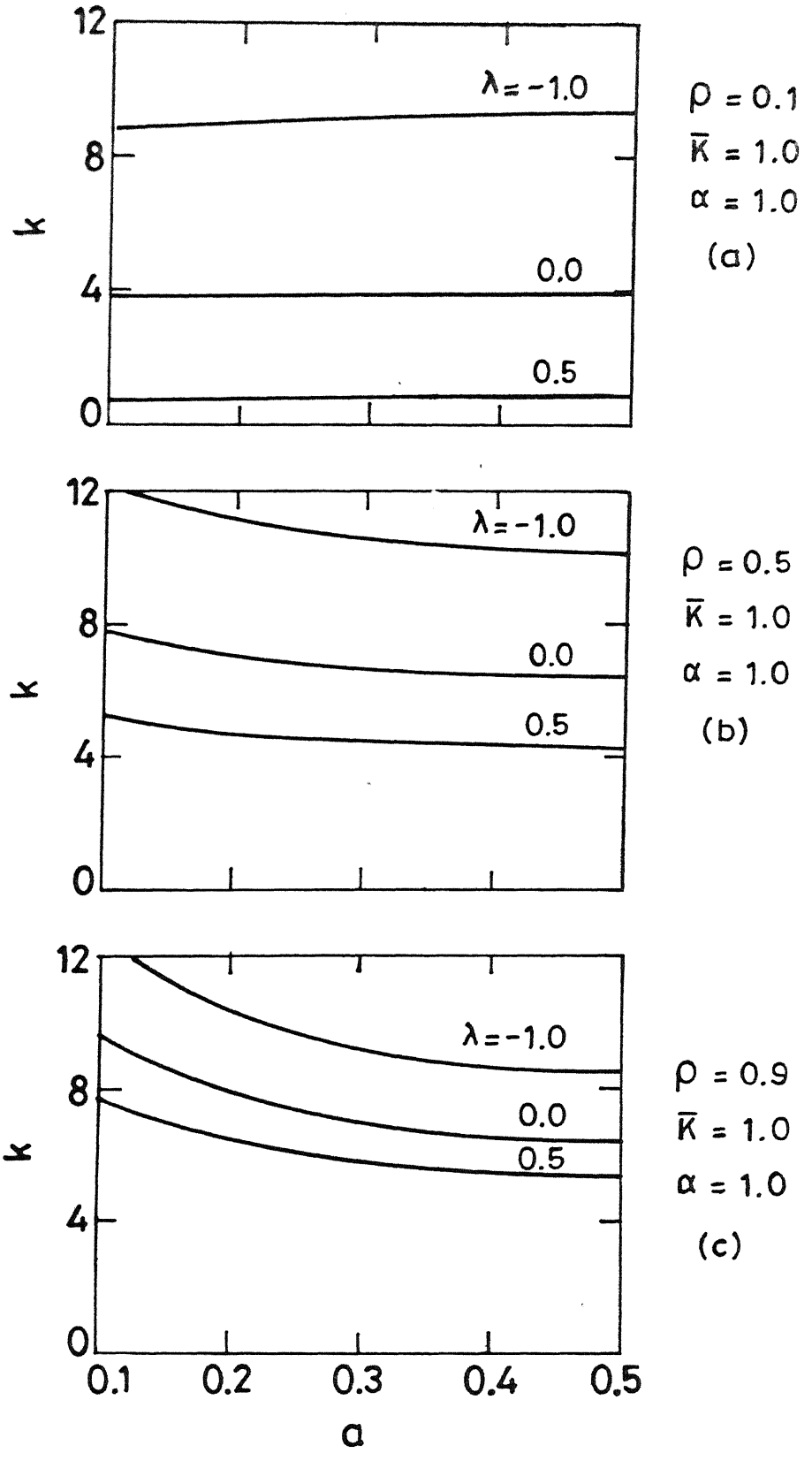

Fig. 3.14 Influence of load position along span on buckling capacity for single point load case (SC)

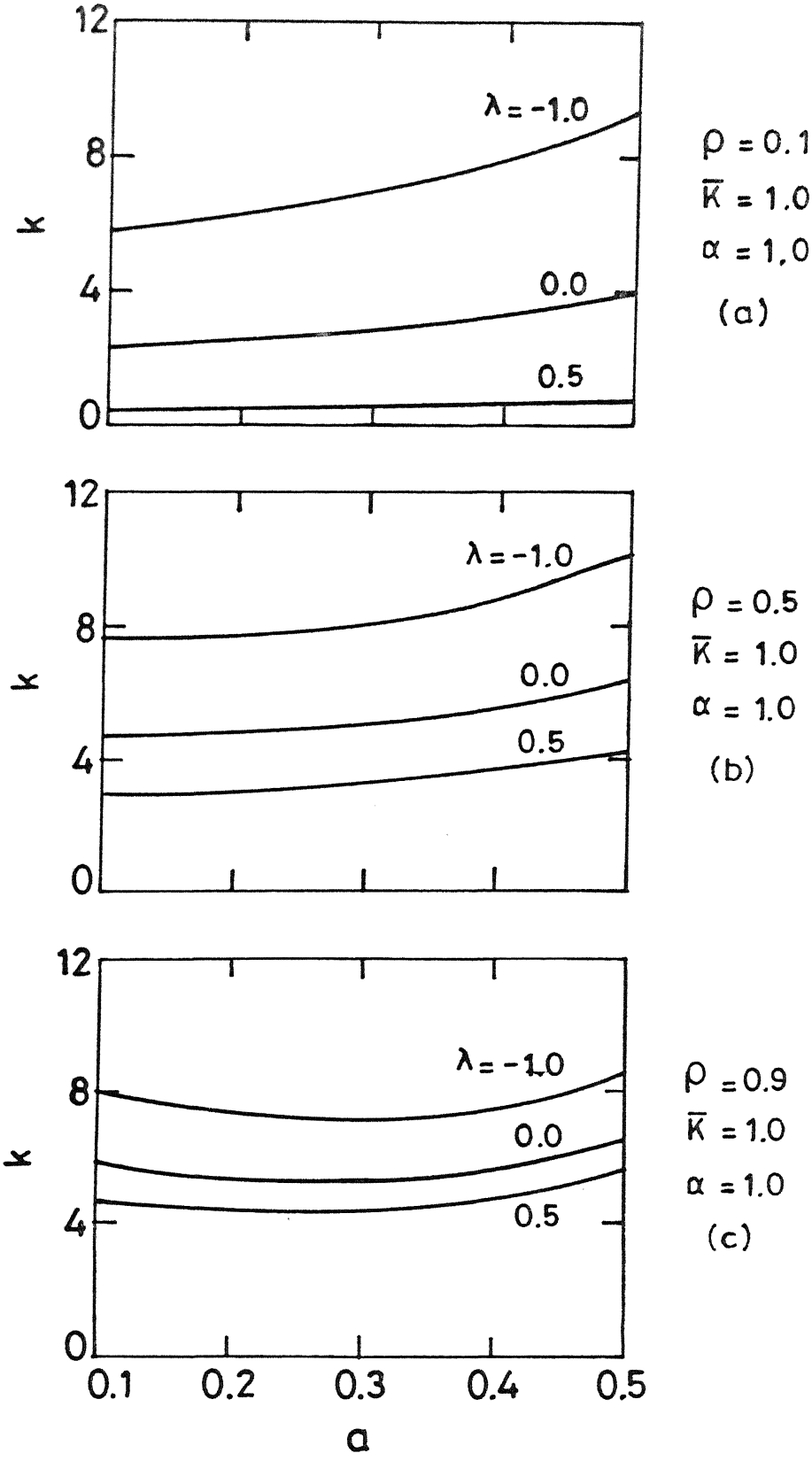

Fig. 3.15 Influence of load position along span on buckling capacity for two point load case (SC).

Table 3.1

Value of f_{cb} based on present analysis and IS:800 for prismatic beam under uniform sagging moment.

l/r_y	ρ = 0.1		ρ = 0.3		ρ = 0.5		ρ = 0.7		ρ = 0.9	
	Present	IS:800	Present	IS:800	Present	IS:800	Present	IS:800	Present	IS:800
100	355.77	534.77	301.92	335.17	365.05	419.43	511.98	493.03	806.16	591.24
125	298.85	449.05	227.73	260.63	258.30	298.81	362.17	345.84	587.10	408.25
150	258.81	387.52	184.07	214.90	198.30	230.69	277.43	263.33	458.98	306.61
175	228.67	340.99	155.30	182.98	160.59	187.63	223.89	211.63	375.73	243.40
200	205.00	304.49	134.81	160.90	134.91	158.18	187.32	176.58	317.60	200.93
225	185.86	275.07	119.41	143.40	116.39	136.82	160.90	151.40	274.82	170.70
250	170.03	250.84	107.36	129.89	102.41	120.65	140.97	132.49	242.09	148.20
275	156.70	230.54	97.64	118.13	91.50	107.98	125.42	117.80	216.26	130.85
300	145.33	213.27	89.61	108.67	82.74	97.77	112.95	106.06	195.37	117.10

Table 3.2

Value of f_{cb} based on present analysis and IS:800 for prismatic, doubly symmetric beams under various transverse loads.

l/r_y	IS:800	Present Analysis			
		Central Point Load		Uniformly Distributed Load	
		TF Load	BF Load	TF Load	BF Load
100	419.43	325.49	756.88	291.45	585.20
125	298.81	239.03	515.67	212.96	400.85
150	230.69	189.86	382.40	168.36	298.76
175	187.63	158.45	300.25	139.92	235.66
200	158.18	136.66	245.51	120.24	193.49
225	136.82	120.62	206.85	105.79	163.62
250	120.65	108.27	178.29	94.68	141.49
275	107.98	98.42	156.44	85.85	124.51
300	97.77	90.35	139.23	78.64	111.10

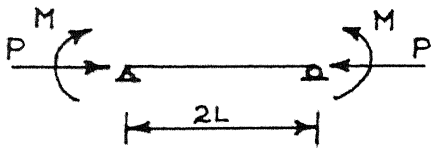

Table 3.3 $\eta = 0.67$ $\alpha = 1.$

$k = 2ML / \sqrt{EI_{yo} GJ_o}$ $\mu = 0.5$ $\rho = 0.$

$\bar{k}$	λ						
	-1.00	-0.50	0.00	0.25	0.50	0.75	1.00
0.25	5.20008	4.46400	3.61238	3.11427	2.53116	1.78157	0
0.50	5.79397	4.87486	3.86013	3.28970	2.64182	1.83625	0
0.75	6.66724	5.49173	4.24100	3.56295	2.81657	1.92394	0
1.00	7.72573	6.25395	4.72290	3.91357	3.04442	2.04038	0
1.25	8.90362	7.11496	5.27823	4.32279	3.31443	2.18097	0
1.50	10.15948	8.04310	5.88624	4.77555	3.61718	2.34137	0
1.75	11.46770	9.01766	6.53223	5.26064	3.94513	2.51779	0
2.00	12.81227	10.02511	7.20601	5.76989	4.29251	2.70710	0

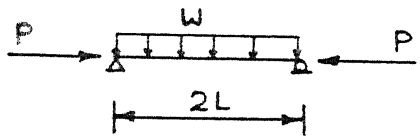

TF Loading

Table 3.4a

$k = wL^3 / \sqrt{EI_{yo} GJ_o}$

$\eta = 0.67$ $\alpha = 1.0$

$\mu = 0.5$ $\rho = 0.5$

$\bar{K}$	λ						
	-1.00	-0.50	0.00	0.25	0.50	0.75	1.00
0.25	5.05414	4.43975	3.69371	3.23755	2.68324	1.93628	0
0.50	5.07347	4.40238	3.62733	3.17013	2.62622	1.90383	0
0.75	5.43848	4.62415	3.73073	3.22783	2.65086	1.91239	0
1.00	6.02282	5.02188	3.95923	3.38225	2.74213	1.95657	0
1.25	6.74293	5.53464	4.27561	3.60779	2.88516	2.03033	0
1.50	7.54902	6.12315	4.65317	3.88473	3.06744	2.12801	0
1.75	8.41164	6.76283	5.07380	4.19894	3.27931	2.24476	0
2.00	9.31289	7.43817	5.52534	4.54051	3.51360	2.37665	0

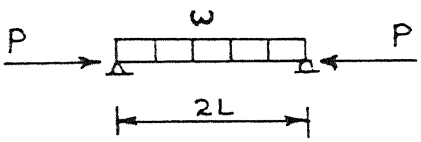

BF Loading

Table 3.4b

$k = wL^3 / \sqrt{EI_{yo} GJ_o}$

$\eta = 0.67$ $\alpha = 1.0$

$\mu = 0.5$ $\rho = 0.5$

$\bar{K}$	λ						
	-1.00	-0.50	0.00	0.25	0.50	0.75	1.00
0.25	6.60377	5.62314	4.49781	3.84644	3.09346	2.14355	0
0.50	8.20234	6.78743	5.24485	4.39419	3.44984	2.31959	0
0.75	10.15148	8.21425	6.16362	5.06817	3.88863	2.53696	0
1.00	12.31894	9.81648	7.20728	5.83875	4.39401	2.78993	0
1.25	14.62097	11.53301	8.33844	6.68022	4.95102	3.07245	0
1.50	17.00814	13.32475	9.53050	7.57292	5.54718	3.37883	0
1.75	19.45126	15.16730	10.76543	8.50275	6.17286	3.70426	0
2.00	21.93262	17.04525	12.03114	9.45985	6.82092	4.04481	0

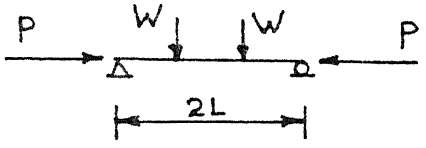

Table 3.5a

$\eta = 0.67 \quad \alpha = 1.0$

$k = \frac{4WL^2}{3} / \sqrt{EI_{yo} GJ_o} \qquad \mu = 0.5 \quad \rho = 0.5$

TF Loading

$\bar{K}$	λ						
	-1.00	-0.50	0.00	0.25	0.50	0.75	1.00
0.25	4.81171	4.23919	3.53937	3.10883	2.58291	1.86961	0
0.50	4.78751	4.16862	3.45001	3.02362	2.51346	1.83044	0
0.75	5.10365	4.35401	3.52882	3.06244	2.52492	1.83172	0
1.00	5.63307	4.71126	3.73043	3.19643	2.60205	1.86807	0
1.25	6.29349	5.18002	4.01772	3.39997	2.72994	1.93346	0
1.50	7.03646	5.72182	4.36433	3.65353	2.89617	2.02227	0
1.75	7.83351	6.31278	4.75254	3.94321	3.09118	2.12970	0
2.00	8.66743	6.93789	5.17051	4.25932	3.30795	2.25188	0

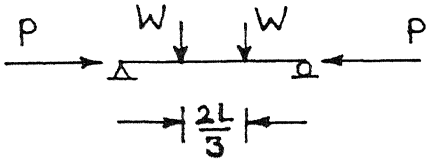

Table 3.5b

$\eta = 0.67 \quad \alpha = 1.0$

$k = \frac{4WL^2}{3} / \sqrt{EI_{yo} GJ_o} \qquad \mu = 0.5 \quad \rho = 0.5$

BF Loading

$\bar{K}$	λ						
	-1.00	-0.50	0.00	0.25	0.50	0.75	1.00
0.25	6.43161	5.48062	4.38633	3.75183	3.01702	2.08952	0
0.50	8.05152	6.66642	5.15141	4.31422	3.38405	2.27109	0
0.75	10.01745	8.11216	6.08700	5.00224	3.83293	2.49353	0
1.00	12.19602	9.72946	7.14531	5.78542	4.34752	2.75106	0
1.25	14.50456	11.45762	8.28898	6.63795	4.91275	3.03759	0
1.50	16.89488	13.25832	9.49171	7.54033	5.51623	3.34750	0
1.75	19.33874	15.10785	10.73585	8.47871	6.14844	3.67601	0
2.00	21.81911	16.99128	12.00963	9.44344	6.80234	4.01925	0

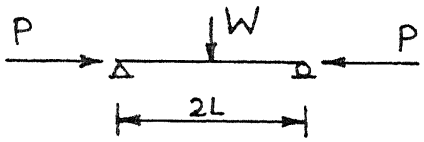

TF Loading

Table 3.6a

$k = WL^2 / \sqrt{EI_{yo} GJ_o}$

$\eta = 0.67$ $\alpha = 1.0$

$\mu = 0.5$ $\rho = 0.5$

$\bar{K}$	λ = -1.00	-0.50	0.00	0.25	0.50	0.75	1.00
0.25	5.70560	5.08399	4.30268	3.80930	3.19332	2.33588	0
0.50	5.63593	4.95944	4.15917	3.67482	3.08437	2.27373	0
0.75	5.98613	5.15630	4.23114	3.70091	3.08110	2.26448	0
1.00	6.59234	5.56268	4.45565	3.84645	3.16107	2.29993	0
1.25	7.35481	6.10403	4.78575	4.07863	3.30499	2.37232	0
1.50	8.21545	6.73345	5.18867	4.37285	3.49701	2.47442	0
1.75	9.14031	7.42202	5.64246	4.71170	3.72504	2.60011	0
2.00	10.10889	8.15161	6.13257	5.08312	3.98019	2.74443	0

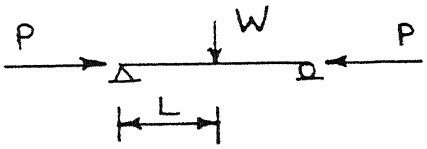

BF Loading

Table 3.6b

$k = WL^2 / \sqrt{EI_{yo} GJ_o}$

$\eta = 0.67$ $\alpha = 1.0$

$\mu = 0.5$ $\rho = 0.5$

$\bar{K}$	λ = -1.00	-0.50	0.00	0.25	0.50	0.75	1.00
0.25	8.03918	6.88615	5.54313	4.75564	3.83555	2.66302	0
0.50	10.20860	8.48781	6.58791	5.52872	4.34385	2.91637	0
0.75	12.78581	10.39995	7.83960	6.45554	4.95303	3.22020	0
1.00	15.62242	12.52413	9.24535	7.50283	5.64606	3.56896	0
1.25	18.61892	14.78620	10.75872	8.63827	6.40400	3.95511	0
1.50	21.71614	17.13844	12.34638	9.83686	7.21077	4.37131	0
1.75	24.87927	19.55125	13.98593	11.08085	8.05406	4.81135	0
2.00	28.08730	22.00603	15.66249	12.35795	8.92483	5.27018	0

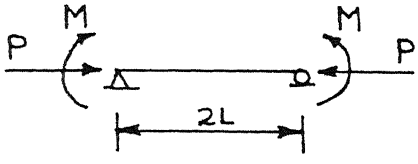

Table 3.7

$k = 2ML / \sqrt{EI_{yo} GJ_o}$

$\eta = 0.67$ $\alpha = 0.5$

$\mu = 0.5$ $\rho = 0.5$

$\bar{K}$	λ						
	-1.00	-0.50	0.00	0.25	0.50	0.75	1.00
0.25	5.20211	4.38668	3.45385	2.91526	2.29289	1.50778	-0.27506
0.50	5.85238	4.80005	3.63595	2.98446	2.25128	1.35704	-0.54917
0.75	6.69797	5.36097	3.91850	3.13105	2.26445	1.23870	-0.82284
1.00	7.68919	6.03595	4.28189	3.34131	2.32374	1.14824	-1.09642
1.25	8.78415	6.79522	4.70768	3.60196	2.42053	1.08114	-1.37002
1.50	9.95220	7.61575	5.18061	3.90156	2.54710	1.03318	-1.64366
1.75	11.17217	8.48087	5.68898	4.23105	2.69707	1.00068	-1.91732
2.00	12.42966	9.37886	6.22413	4.58349	2.86537	0.98060	-2.19100

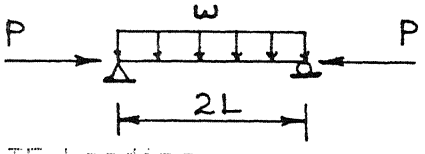

TF Loading

Table 3.8

$k = wL^3 / \sqrt{EI_{yo} GJ_o}$

$\eta = 0.67$ $\alpha = 0.5$

$\mu = 0.5$ $\rho = 0.5$

$\bar{K}$	λ						
	-1.00	-0.50	0.00	0.25	0.50	0.75	1.00
0.25	5.16830	4.44222	3.58101	3.06627	2.45330	1.64936	-0.31764
0.50	5.27703	5.45073	3.49497	2.93482	2.27679	1.42517	-0.63450
0.75	5.59588	4.62962	3.53734	2.90942	2.18234	1.25557	-0.95100
1.00	6.07447	4.94005	3.68054	2.96810	2.15361	1.13014	-1.26744
1.25	6.66833	5.34733	3.89968	3.09088	2.17563	1.03931	-1.58389
1.50	7.34382	5.82444	4.17472	3.26138	2.23594	0.97493	-1.90037
1.75	8.07741	6.35198	4.49082	3.46730	2.32495	0.93063	-2.21687
2.00	8.85301	6.91638	4.83735	3.69966	2.43560	0.90161	-2.53339

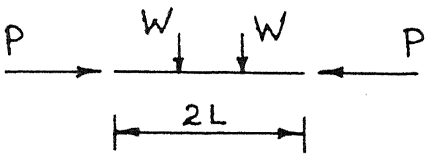

TF Loading

Table 3.9

$k = \frac{4WL^2}{3} / \sqrt{EI_{yo} GJ_o}$

$\eta = 0.67$ $\alpha = 0.5$

$\mu = 0.5$ $\rho = 0.5$

$\bar{K}$	λ						
	-1.00	-0.50	0.00	0.25	0.50	0.75	1.00
0.25	4.93670	4.25520	3.44141	2.95220	2.36697	1.59531	-0.30867
0.50	5.00107	4.23399	3.33955	2.81158	2.18772	1.37452	-0.61671
0.75	5.27363	4.38166	3.36508	2.77625	2.09002	1.20805	-0.92446
1.00	5.70242	4.65832	3.48982	2.82380	2.05722	1.08531	-1.23215
1.25	6.24307	5.02927	3.68877	2.93411	2.07426	0.99663	-1.53985
1.50	6.86257	5.46788	3.94207	3.09095	2.12870	0.93386	-1.84757
1.75	7.53799	5.95518	4.23515	3.28216	2.21107	0.89069	-2.15531
2.00	8.25377	6.47798	4.55763	3.49896	2.31443	0.86237	-2.46307

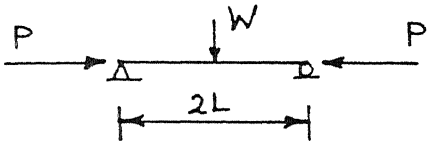

TF Loading

Table 3.10

$k = WL^2 / \sqrt{EI_{yo} GJ_o}$

$\eta = 0.67$ $\alpha = 0.5$

$\mu = 0.5$ $\rho = 0.5$

$\bar{F}$	λ						
	-1.00	-0.50	0.00	0.25	0.50	0.75	1.00
0.25	5.74221	5.01493	4.12193	3.57034	2.89486	1.97802	-0.39286
0.50	5.68607	4.88077	3.91966	3.33772	2.63324	1.68883	-0.78571
0.75	5.90943	4.97821	3.89567	3.25369	2.48735	1.46787	-1.17857
1.00	6.32614	5.23875	4.00020	3.27843	2.42780	1.31020	-1.57143
1.25	6.87767	5.61511	4.19799	3.38310	2.43263	1.19723	-1.96429
1.50	7.52306	6.07336	4.46296	3.54598	2.48491	1.11769	-2.35714
1.75	8.23449	6.58998	4.77652	3.75132	2.57215	1.06306	-2.75000
2.00	8.99333	7.14887	5.12568	3.98799	2.68538	1.02707	-3.14286

REFERENCES

1. Bradford, M.A., and Cuk, P.E. (1988). "Elastic buckling of tapered monosymmetric I-beams." J. Struct. Engrg., ASCE, 114 (5), 977-996.

2. Brown, T.G. (1981). "Lateral torsional buckling of tapered I-beams." J. Struct. Div., ASCE, 107 (ST4), 689-697.

3. Chajes, A. (1974). Principles of structural stability theory. Prentice Hall, Inc., N.J.

4. Culver, C.G., and Preg., S.M. (1968). "Elastic stability of tapered beam-columns." J. Struct. Div., ASCE, 94(ST2), 455-470.

5. Fogel, C.M., and Ketter, R.L. (1962). "Elastic strength of tapered columns." J. Struct. Div., ASCE, 88 (ST5), 67-106.

6. Galambos, T.V. (1968). Structural members and frames. Prentice Hall, Inc., N.J.

7. Gere, J.M., and Carter, W.O. (1962). "Critical buckling loads for tapered columns." J. Struct. Div., ASCE, 88 (ST1), 1-11.

8. Girijavallabhan, C.V. (1969). "Buckling loads of non-uniform columns." J. Struct. Div., ASCE, 95 (ST 11), 2419-2431.

9. IS:800 (1984). Code of practice for general construction in steel. Indian Standards Institution, New Delhi.

10. Kitipornchai, S., and Trahair, N.S. (1972). "Elastic behaviour of tapered I-beams." J. Struct. Div., ASCE, 98 (ST 3), 713-728.

11. Kitipornchai, S., and Trahair, N.S. (1975). "Elastic behaviour of tapered monosymmetric I-beams." J. Struct. Div., ASCE, 101 (ST 8), 1661-1678.

12. Kitipornchai, S., and Trahair, N.S. (1980). "Buckling of monosymmetric beams." J. Struct. Div., ASCE, 106 (ST 5), 941-957.

13. Kitipornchai, S., and Trahair, N.S. (1986a). "Buckling of monosymmetric I-beams under moment gradient." J. Struct. Engrg., ASCE, 112 (4), 781-799.

14. Kitipornchai, S., and Wang, C.M. (1988a). "Out of plane buckling formulae for beam-columns/tie-beams." J. Struct. Engrg., ASCE, 114 (12), 2773-2789.

15. Kitipornchai, S., and Wang, C.M. (1988b). "Flexural-torsional buckling of monosymmetric beam-columns/tie-beams." Struct. Eng., 66 (23), 393-399.

16. Lee, G.C., and Szabo, B.A. (1967). "Torsional response of tapered I-girders." J. Struct. Div., ASCE, 93 (ST 5), 233-252.

17. Timoshenko, S.P., and Gere, J.M. (1961). Theory of elastic stability. McGraw Hill, New York.

18. Trahair, N.S., and Bradford, M.A. (1988). The behaviour and design of steel structures, Chapman and Hall, London.

19. Wang, C.M., and Kitipornchai, S. (1986b). "Buckling capacities of monosymmetric I-beams." J. Struct. Engrg., ASCE, 112 (11), 2373-2391.

20. Wang, C.M., and Kitipornchai, S. (1989). "New set of parameters for monosymmetric beam-columns/tie-beams." J. Struct. Engrg., ASCE, 115 (6), 1497-1513.